UNIVERSIDADE D
COIMBRA

STEPAN BOBROVNIKOV

# STUDY OF CAVITATION EROSION PROCESS TO EVALUATE THE INTEGRITY OF WC COMPOSITES OBTAINED BY POWDER METALLURGY.

**VOLUME 1**

**Dissertation is prepared within the scope of the Erasmus Mundus Joint Master's Degree "Tribology of Surfaces and Interfaces" supervised by Doctor Luís Miguel Cardoso Vilhena Pereira da Silva and Professor Amílcar Lopes Ramalho**

**Department of Mechanical Engineering of the Faculty of Science and Technology**

Julho de 2022

FACULDADE DE CIÊNCIAS E TECNOLOGIA
UNIVERSIDADE D COIMBRA

# Study of cavitation erosion process to evaluate the integrity of WC composites obtained by powder metallurgy

Submitted in Partial Fulfilment of the Requirements for the Degree of European Joint European Master in Tribology of Surfaces and Interfaces.

# Estudo do processo de erosão por cavitação para avaliar a integridade de compósitos de WC obtidos por metalurgia do pó


**Author**

**Stepan Bobrovnikov**

**Advisor[s]**

**Dr. Luís Miguel Cardoso Vilhena Pereira da Silva**

**Prof. Amílcar Lopes Ramalho**


| | |
|---|---|
| **President** | **Professor Bruno Miguel Quelhas de Sacadura Cabral Trindade** |
| | **Professor at the Universidade de Coimbra** |
| **Vowel** | **Professor Albano Augusto Cavaleiro Rodrigues de Carvalho** |
| | **Professor at Universidade de Coimbra** |
| **Advisor** | **Doutor Luís Miguel Cardoso Vilhena Pereira da Silva** |
| | **Professor at Universidade de Coimbra** |

UNIVERSIDADE D COIMBRA

tribos

**Jury**

**Coimbra, July, 2022**

# ACKNOWLEDGEMENTS

I would like to express my gratitude to all who have contributed to completing the project described in this thesis.

First and foremost, I would like to thank my advisors, Prof. Amílcar Lopes Ramalho and Dr. Luís Miguel Cardoso Vilhena Pereira da Silva from the University of Coimbra, for their guidance and valuable input during the project. I am grateful for the their time spent and continues support given within the project, which let me develop unique engineering skills and enrich my knowledge.

Special thanks to the TRIBOS consortium for providing me with this life-changing opportunity and the European Commission's funding. I wish well for my TRIBOS mentors Professor Ardian Morina, Professor Mitjan Kalin, Doctor Muhammad Shahid Arshad and Professor Bruno Trindade for their support.

Finally, I want to express my profound gratitude to my parents, family, and friends who have offered constant support and encouragement, directly or indirectly, throughout this degree and while writing this thesis.

# Abstract

One of the typical causes of degradation of machinery components in a fluid flow is the cavitation-erosion [1]. Component failure is caused by material removal due to exposure to the repetitive implosion of air bubbles called cavities to the component's surface [2].

Cavitation-erosion is a phenomenon of complex nature, which includes properties and hydrodynamic factors of liquid, as well as properties of the solid body exposed to the cavitation erosion as microstructure, surface properties as hardness, and properties of bulk material as density, Young modulus, etc.

Design and definition of service parameters of many machinery components such as water turbines' blades, control valves, curved sections of pipelines, rotors of centrifugal pumps, etc. exposed to cavitation effect require well-defined test methods to evaluate cavitation-erosion and estimate cavitation-erosion resistance properties of materials. Several test methods based on cavitation-erosion were developed for these purposes, results are used for the evaluation of cavitation-erosion resistance of specific materials.

The objective of undertaken work is the cavitation-erosion resistance calculation of several sintered composites and improvement of existing cavitation-erosion testing method. Suggested method could be used for quality assessment of composed material and different manufacturing method, for example comparison of sintered components and components produced by additive manufacturing using the same material composition. The alternative method of additive manufacturing still raises many problems due to the typical defects such as undesired porosity and cracking, which potentially have a significant effect on cavitation-erosion resistance of the material.

In the present research work, cavitation-erosion resistance of the following material produced with conventional powder metallurgy method has been analyzed: WC-Co, WC-Ni, WC-CoNi, WC-CoCr, WC-NiCr, WC-CoNiCr and WC-NiCrMo. The comparison of materials' cavitation-erosion resistance values let us choose the best material in relation to resistance to cavitation erosion, comparison of different binders reveal different erosion mechanisms, what also provides the data for further comparison with additive manufactured material with the same composition.

***Keywords:*** *WC-based composites, hardmetals, cavitation-erosion, wear resistance, binders*

# Resumo

Uma das causas típicas de degradação de componentes de máquinas em um fluxo de fluido é a erosão provocada por cavitação [1]. A falha do componente é causada pela remoção de material devido à exposição à implosão repetitiva de bolhas de ar chamadas cavidades na superfície do componente [2].

A erosão por cavitação é um fenômeno de natureza complexa, que inclui propriedades e fatores hidrodinâmicos do líquido, bem como propriedades do corpo sólido exposto à erosão por cavitação como microestrutura, propriedades de superfície como dureza e propriedades do material a granel como densidade, módulo de Young, etc.

Projeto e definição de parâmetros de serviço de muitos componentes de máquinas, como pás de turbinas hidráulicas, válvulas de controle, seções curvas de tubulações, rotores de bombas centrífugas e etc. expostos ao efeito de cavitação requerem métodos de teste bem definidos para avaliar a erosão provocada por cavitação e estimar as propriedades de resistência dos materiais à erosão por cavitação. Vários métodos de ensaio baseados na erosão por cavitação foram desenvolvidos para estes fins, os resultados são utilizados para a avaliação da resistência à erosão por cavitação de materiais específicos.

O objetivo do trabalho realizado é o cálculo da resistência à erosão por cavitação de vários compósitos sinterizados e melhoria do método de teste de erosão por cavitação existente. O método sugerido pode ser usado para avaliação de qualidade de material composto e método de fabricação diferente, por exemplo, comparação de componentes sinterizados e componentes produzidos por manufatura aditiva usando a mesma composição de material. O método alternativo de manufatura aditiva ainda gera muitos problemas devido aos defeitos típicos, como porosidade indesejada e trincas, que potencialmente têm um efeito significativo na resistência à erosão por cavitação do material.

Na presente pesquisa, foi analisada a resistência à erosão por cavitação dos seguintes materiais produzidos pelo método convencional da metalurgia do pó: WC-Co, WC-Ni, WC-CoNi, WC-CoCr, WC-NiCr, WC-CoNiCr e WC-NiCrMo. A comparação dos valores de resistência à erosão por cavitação dos materiais permite-nos escolher o melhor material em relação à resistência à erosão por cavitação, a comparação de diferentes ligantes revela diferentes mecanismos de erosão, o que também fornece dados para posterior comparação com material fabricado aditivado com a mesma composição.

**Palavras-chave:** Compósitos à base de WC, metais duros, cavitação-erosão, resistência ao desgaste, ligantes

# Contents

Abstract ..... ii

Resumo ..... iii

[LIST OF SIMBOLS] AND [ACRONYMS/ ABBREVIATIONS] ..... ix

[List of Symbols] ..... ix

[Acronyms/Abbreviations] ..... ix

1. Introduction ..... 1

2. State of the Art ..... 3

2.1 Cavitation erosion ..... 3

2.2 Consequences of cavitation and the importance of its study ..... 4

2.3 Cavitation induction ..... 5

2.4 Cavitation erosion detection and methods of reduction ..... 8

3. Materials and methods ..... 9

3.1 Ultrasonic cavitation-erosion equipment ..... 9

3.2 Resonance frequency of the grain ..... 10

3.3 Experimental protocol ..... 12

3.4 Specimens characterization ..... 14

4. Results and discussion ..... 18

4.1 3D laser profilometer measurements ..... 18

4.2 Grain size estimation using FFT ..... 28

4.3 SEM analysis ..... 29

4.4 EDS compositional analysis ..... 30

4.5 Subsurface hardening ..... 35

5. Conclusion ..... 36

6. Future work ..... 37

References ..... 38

[LIST OF FIGURES]

**Figure 1.** Phase diagram with two transition Liquid-Vapor routes caused by boiling and cavitation [4]. .....1
**Figure 2.** Cavitation collapse shock wave mechanism [7]. .....2
**Figure 3.** Classification scheme for the different kinds of cavitation [21]. .....5
**Figure 4.** Apparatus to hydrodynamic cavitation study [23]. .....6
**Figure 5.** Ultrasonic cavitation equipment [25]. .....7
**Figure 6.** Optical cavitation system representation [26]. .....8
**Figure 7.** Ultrasonic cavitation-erosion equipment. .....9
**Figure 8.** Transducer connected with the ultrasonic horn. .....10
**Figure 9.** Fisher Scientific Sonic Dismembrator Model 500. .....10
**Figure 10.** Schematic of WC grain attached to the surface with binder neck. .....11
**Figure 11.** Dimensions of the counterbody. .....13
**Figure 12.** WC particle distribution (source: DURIT hartmetall). .....16
**Figure 13.** Square indentation of 136 degree pyramid with corresponding measurements. .....17
**Figure 14.** 3D profile from the surface of WC-Co, after 24 hours of cavitation-erosion cycle. .....18
**Figure 15.** Evolution of 2D profile of WC-Co. .....19
**Figure 16.** Evolution of volume loss: a) all specimens: b) WC-Co excluded. .....20
**Figure 17.** Evolution of volume loss rate: a) all specimens; b) WC-Co excluded. .....22
**Figure 18.** Evolution of volume loss and volume loss rate for the WC-Co specimen. .....22
**Figure 19.** Evolution of volume loss and volume loss rate for the WC-Ni specimen. .....23
**Figure 20.** Evolution of volume loss and volume loss rate for the WC-CoNi specimen. .....23
**Figure 21.** Evolution of volume loss and volume loss rate for the WC-CoCr specimen. .....23
**Figure 22.** Evolution of volume loss and volume loss rate for the WC-NiCr specimen. .....24
**Figure 23.** Evolution of volume loss and volume loss rate for the WC-CoNiCr specimen. .....24
**Figure 24.** Evolution of volume loss and volume loss rate for the WC-NiCrMo specimen. .....24
**Figure 25.** Volume loss chart and cavitation erosion rate calculation WC-Co .....25
**Figure 26.** Volume loss chart and cavitation erosion rate calculation WC-Ni .....25
**Figure 27.** Volume loss chart and cavitation erosion rate calculation WC-CoNi .....26
**Figure 28.** Volume loss chart and cavitation erosion rate calculation WC-CoCr .....26
**Figure 29.** Volume loss chart and cavitation erosion rate calculation WC-NiCo .....26
**Figure 30.** Volume loss chart and cavitation erosion rate calculation WC-CoNiCr .....27
**Figure 31**. Volume loss chart and cavitation erosion rate calculation WC-NiCrMo .....27

**Figure 32.** FFT of WC-Cospecimen profile: a) before cavitation-erosion; b) after cavitation-erosion. .....28
**Figure 33.** Cavitation-erosion pit on the surface of WC-Co specimen. .....29
**Figure 34.** SEM image of eroded area of WC-Co specimen. .....30
**Figure 35.** EDS line scan over WC-CoCr eroded surface. .....31
**Figure 36.** EDS over WC-CoCr eroded surface: (a) line scan compositional analysis: (b) EDS spectra. .....32

[LIST OF TABLES]

**Table 1.** Nominal composition of the prepared hardmetal grades. .....14
**Table 2.** Surface roughness parameters for the different hardmetal grades. .....15
**Table 3.** Mechanical properties for the different hardmetal grades. .....16
**Table 4.** Erosion rates of the different specimens at the different stages.....27

# [LIST OF SIMBOLS] AND [ACRONYMS/ ABBREVIATIONS]

## [List of Symbols]

$\nu$ – frequency

k – spring constant

m – mass

$\pi$ – Pi number

F – force

A – indentation area

d – average length of indentation diagonals

P – load

T – crack length

E – Young's modulus

S – surface area

V – volume

l – length

$\rho$ – density

## [Acronyms/Abbreviations]

ASTM – American Society for Testing and Materials

SEM – Scanning Electron Microscopy

WC – Tungsten carbide

Co – Cobalt

Cr – Chromium

Ni – Nickel

Mo – Molybdenum

HVOF – High-Velocity Oxygen Fuel

HV – The Vickers Hardness

ISO – International Organization for Standardization

$KIC$ – Fracture toughness

FFT – Fast-Fourier Transform

EDS – Energy Dispersive Spectroscopy

# 1. Introduction

ASTM defines cavitation as the formation and subsequent collapse of vapor or gas bubbles within a liquid, caused, in general, by a local pressure decrease [3]. Both cavitation and boiling are associated with gas bubbles formation within the liquid, but the definition of cavitation distinguishes it from boiling, which causes the formation of vapor bubbles due to an increase in the temperature of the liquid. The difference explained could be represented the best with a phase diagram presented in Figure 1. The transition from liquid to vapor phase could be achieved through two different mechanisms: temperature increase provides vapor formation by boiling, pressure decrease leads to cavitation.

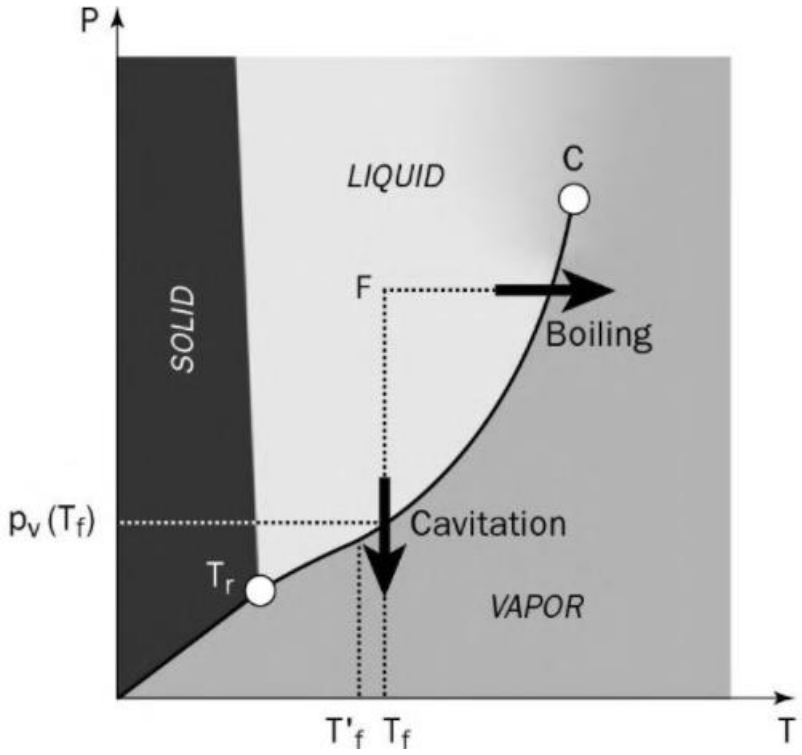


**Figure 1.** Phase diagram with two transition Liquid-Vapor routes caused by boiling and cavitation [4].

Transient isolated bubbles is the most common form of cavitation. The bubbles appear as a very small air nuclei growth in the low-pressure regions in the liquid [4]. The formation of the low-pressure regions is the key aspect for cavitation formation, there are several typical situations when low-pressure regions could be developed: streamlines with cross-sectional area decrease or curved geometry create rapid local velocity increase what resulting local pressure drop; local roughness, shear, and unsteady flows create large turbulent pressure fluctuations causing cavitation formation [5]. Another favorable situation for cavitation formation is vibration, which creates an oscillation pressure field. Cavitation formation imposed by vibration is used for the cavitation erosion test method used in this work.

Dynamics of the cavitation bubble collapse is ruled by pressure distribution around the bubble. If the bubble is located in close proximity to the solid boundary, it has two zones: a zone of lower pressure on the side next to the solid surface and a zone of high pressure on the opposite side. Therefore, the spherical bubble perturbs and collapses inside from the side of the high pressure – side more distant from the solid surface (Figure 2). Asymmetrical collapse creates microjets of high pressure directed right against the surface, which causes severe surface deterioration and material loss.

It is crucial in components design that cavitation effects are considered. When a cavitation bubble collapses - it creates a pressure wave. When the cavitation bubble collapses next to the solid boundary it also creates additional stress on the surface due to asymmetrical collapse, what can increase destructive effects of cavitation [6].

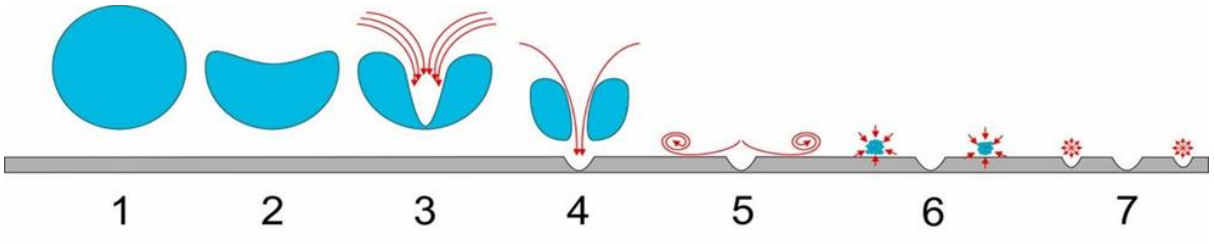


**Figure 2.** Cavitation collapse shock wave mechanism [7].

The main goal of the proposed thesis is to perform quantitative analysis of cavitation erosion resistance of several materials. The analysis includes determination of the wear volume induced by cavitation erosion, based on material loss rate, surface roughness evolution, profile evolution from the wear scar. Analysis of material removal mechanism is provided based on Optical Microscopy (OM) and Scanning Electron Microscopy (SEM) analysis. 2D and 3D profiles were also obtained by profilometry techniques. All together quantitative and qualitative means of analysis provide a detailed overview of cavitation erosion resistance of analyzed materials.

The scope of the work is an analysis of seven different WC-based composites with different binders: WC-Co, WC-Ni, WC-CoNi, WC-CoCr, WC-NiCr, WC-CoNiCr and WC-NiCrMo. Materials of the group of WC cemented carbides are compared to each other to define the best performing material in relation to cavitation erosion resistance.

All the collected data on cavitation erosion resistance is going to be used in the further research, what includes analysis of materials with the same composition produced by laser powder bed fusion additive manufacturing technique. The comparison of cavitation erosion resistance of materials with the same composition produced with different methods can reveal manufacturing defects as well as establish a quality assessment method suitable for materials produced in different methods.

# 2. State of the Art

## 2.1 Cavitation erosion

Cavitation erosion is a complex phenomenon, which depends on the physical, mechanical, and microstructural properties of both liquid and solid material. There are several theoretical works published, explaining the phenomenon of cavitation as well as experimental works presenting a quantitative analysis of cavitation erosion resistance of different materials.

Zakrzewska and Krella [2] in their work presented a correlation of specific mechanical properties (hardness, yield strength, tensile strength, fatigue strength, and strain energy) with cavitation erosion resistance. With the simplicity of correlation relations, it was shown that hardness, ultimate tensile strength, yield strength have an exponential correlation with cavitation erosion resistance, but hardness increase leads to brittleness increasing and for brittle materials, it leads to lower cavitation erosion resistance.

Slaza and Hejwowski have proposed wear mechanism and cavitation erosion resistance comparison for $Al_2O_3$-40%$TiO_2$/NiMoAl cermet coatings produced by Flame Spraying. Authors have compared different compositions of the coating and also investigated relations of porosity, surface roughness parameters on cavitation erosion resistance [8].

Tzanakis et al. have researched the cavitation erosion behavior of commercial grades of steel. It was shown that crack propagation during the brittle failure mode of the surface takes place preferentially along the grain boundary [9]. Grain size has also been shown an important parameter influencing cavitation erosion rate, it was shown that removal of bigger grains leads to a higher erosion rate.

In the present research work, the analysis of the erosion effect induced by cavitation on WC-based composites with different binders is carried out, as it was just a few works [10-12] that highlight cavitation erosion resistance of this group of materials. Ding et al. [10] have shown that HVOF-prepared nanostructured WC–12Co coating performs excellent cavitation erosion resistance. Du et al. [11] have performed several measurements of WC-12Co coatings and found a relation of cavitation rate with micro defects of the coating, it was shown that these defects lead to propagation and connection of the cracks and pores of the coating, what is the dominant cause of the decrease of cavitation erosion resistance.

## 2.2 Consequences of cavitation and the importance of its study

Normally, the phenomenon of cavitation is unwanted due to its negative impacts such as system malfunction, material degradation, noise, and unwanted vibration.

Erosion is the material degradation type, caused by the impact of solid, liquid, or gaseous particles against the surface of the material. In case of cavitation erosion, shock waves and microjets are formed by collapsing bubbles next to material surfaces providing erosive wear [13].

In the beginning, cavitation damage was related to the hardness of the material. Early works suggested relating the mechanical properties of structurally identical materials to the level of damage caused by cavitation [14]. It was found that the cavitation damage is exponentially proportional to the hardness of the material. Later fatigue strength was suggested to be a property used to define cavitation erosion resistance. It was suggested that the erosion process is caused by cyclic fatigue [15-16]. Later correlation between resistance to fatigue strength and cavitation erosion resistance, measured by the incubation time as well as the rate of mass loss, was found [17].

Another important effect on machinery subjected to cavitation is plastic deformation. Plastic deformation occurs as the dislocation of crystalline planes within a material. The level of stresses required to produce such a dislocation is known as yield strength. Created dislocations in the material are irreversible and it becomes a source of increased tensions in the material crystalline [18]. Shock waves produced by cavitation cause the formation of irregularities, and initial hardening of the material due to the plastic deformation leads to brittle behavior on the surfaces inducing micro-cavities, and micro-cracks on the surface of the material. Also, it is known that ductile materials can fracture in a brittle manner under impulsive loading and hypervelocity regimes [19].

Noise is also one of the cavitation consequences seriously taken into account – more than 83% of all the noise produced by the large marine vessels is composed of propeller cavitation noise [20]. Impulsive pressure of cavitation bubbles also produces vibration of the affected surface, which eventually increases the noise level. Alongside with negative aspects of noise produced from cavitation, several tests method have been developed for hydraulic machine monitoring and assessment.

## 2.3 Cavitation induction

There are several methods used to produce and study cavitation, Lauterborn has performed one of the first systematizations of the methods to group different types of cavitation [21]. Lauterborn's approach is presented in Figure 3.

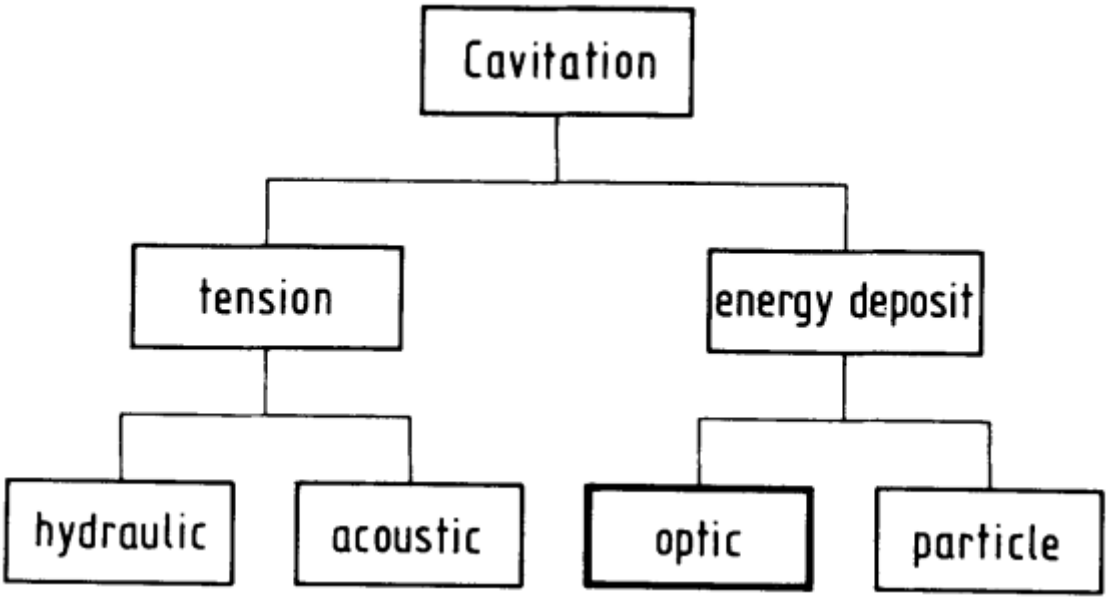


**Figure 3.** Classification scheme for the different kinds of cavitation [21].

According to the scheme provided on the Figure 3, cavitation can be classified by mechanism of it development. First mechanism is tension in the liquid, when cavitation is brought by pressure difference due to hydraulic or acoustic means. Second mechanism is energy deposition, when cavitation is formed by local deposit of energy using optical means or directed by particle deposition.

Hydrodynamic cavitation study was started with first mention by Euler in 1755 by observation of the effect in hydraulic pumps and propellers for naval use [22]. Considering hydrodynamic cavitation, the stress in the liquid is built upon pressure difference originating from velocity variations in the system due to geometric changes and obstacles in the flow.

In accordance with Bernoulli's Law, the increase in flow velocity leads to corresponding pressure reduction and vice versa. In case, the vapor pressure of the liquid is reached, cavitation formation pressure drop occurs. A zone of reduced pressure can occur in the fluid in many cases. Usually, turbulence flows are coming along with cavitation formation due to the continuous appearance of zone low-pressure zones. If the fluid crosses constriction or an obstacle, the low-pressure zone is founded right next to the solid boundary in the flow. Fluid in the flow with cross-section reduction experiencing velocity increase and pressure drop at thinning zone.

In Figure 4 an apparatus to study hydrodynamic cavitation is presented. The apparatus is used to obtain several different measurements to characterize the flow and undergoing processes: flow velocity profile, turbulence, and developing vortices are analyzed, and cavitation, cavitation inception index, and noise spectra are measured [23]. In engineering, the hydrodynamic approach for cavitation research is reliable and useful for the investigation of methods of developing and preventing cavitation formation in a fluid flow. But the reliability of the method comes at the cost of extreme time demand. Material behavior lies in the slow progression of the cavitation damage in comparison to other cavitation investigation methods, what is the main disadvantage of the method, and common reasons for other methods' preferences.

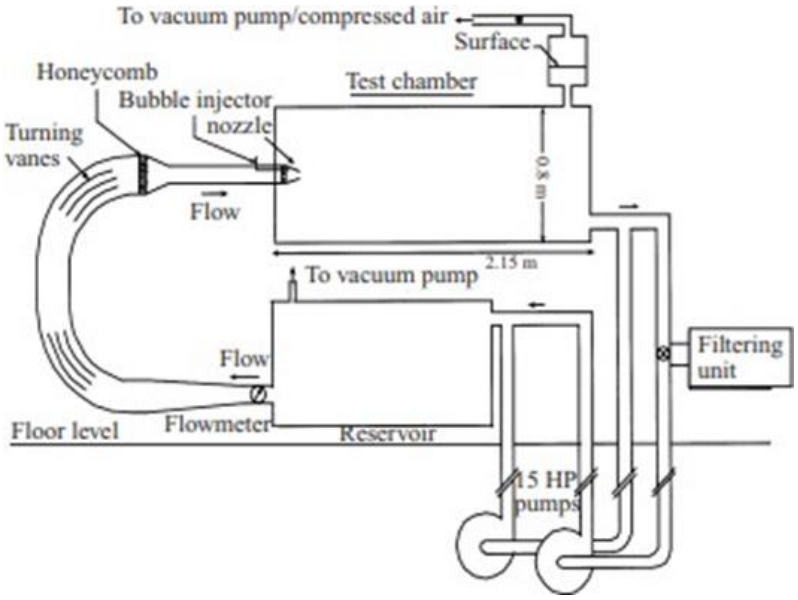


**Figure 4.** Apparatus to hydrodynamic cavitation study [23].

Mentioned disadvantage of extreme time demand of hydrodynamic cavitation method for cavitation damage research suggest application of other methods. In this work acoustic method based on vibratory cavitation through ultrasound is used.

Pressure variation to impose cavitation formation is produced by vibratory movement of ultrasonic horn of ultrasonic equipment. Each cycle involves low and high pressure phases, cavitation bubbles are getting produced and then collapsed each cycle during the low-pressure phase and high-pressure phase, respectively.

Ultrasound is high-frequency waves, which corresponds to a range of frequencies upper human audible limit. Laboratory ultrasound equipment usually has a range between 20 kHz and 100 kHz [24]. The commonly used scheme of ultrasonic cavitation equipment is consist of three main components: an Ultrasonic processor, ultrasonic horn and could be also equipped with a cooling system (Figure 5). An

ultrasonic processor is a source of energy for the process. The energy is getting converted into vibratory movement, directed onto the horn. The horn immersed into the liquid produces pressure cycles, which are generating cavitation. A more detailed explanation of the method is provided in the next section – the experimental procedure.

The main advantage of the acoustic cavitation method is high operation frequencies, which are capable to accelerate the cavitation formation cycle and achieve much higher cavitation erosion damage rates. The same damage produced by hydrodynamic cavitation for a period of weeks can be achieved in hours in the case of acoustic cavitation [25].

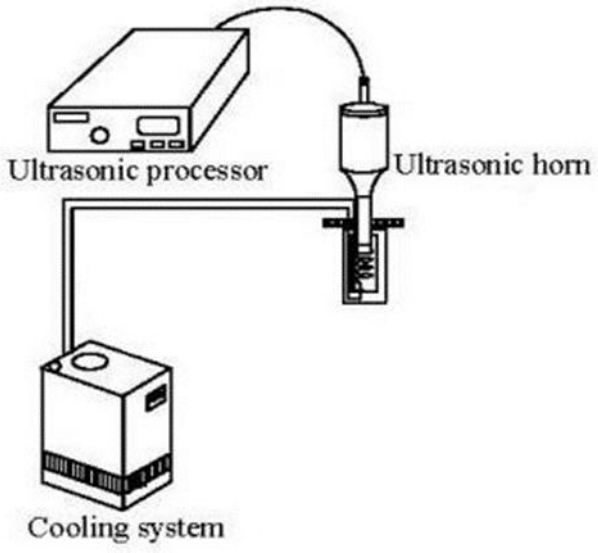


**Figure 5.** Ultrasonic cavitation equipment [25].

Optical and Particle Cavitation method is based on direction of concentration of energy at a certain points to increase local temperature and cause cavitation. It is important to note, that the process is energy and temperature related, so it could be associated with boiling, but as the formation and collapsing of bubbles is localized and the source of the cavitation is not important to study cavitation damage the method is grouped as cavitation method as well.

For optical cavitation, the concentration of energy is achieved by focusing a high-intensity laser at the specific point of liquid using a set of lenses – the common laboratory set for optical cavitation study is presented in Figure 6.

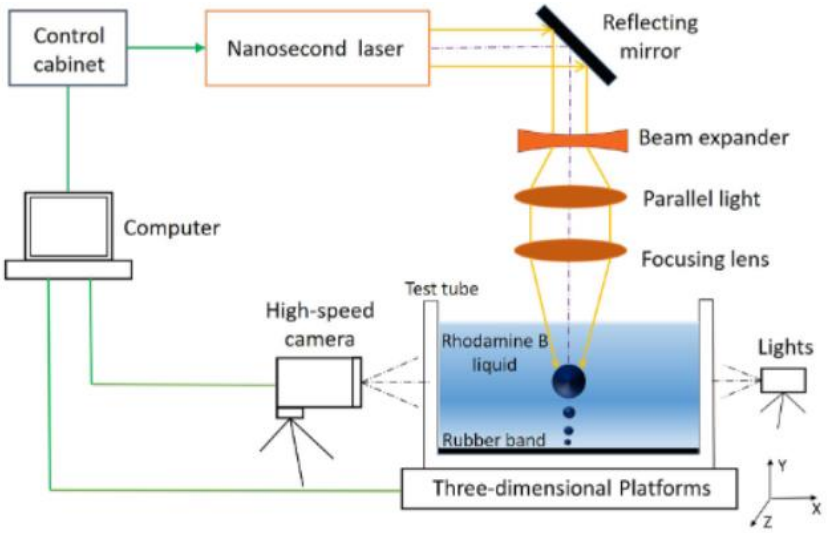


**Figure 6.** Optical cavitation system representation [26].

Particle cavitation is based on the same principle as optical cavitation, but energy is directed using a particle, for example, a photon passing through the liquid. On the way through the liquid photon is interactive with molecules of fluid and releases ions by breaking the liquid. Released ions produce a huge amount of energy via interaction with electrons, which causes a local increase in temperature and cavitation formation.

## 2.4 Cavitation erosion detection and methods of reduction

Usually, cavitation is an undesired effect due to its negative coincidence. In previous sections, some of the negative coincidences of cavitation have been discussed, here is it highlighted that these negative effects of cavitation are used in the instruments for its detection.

Du et al. [11] have shown in their work that surface roughness is positively correlated with cavitation erosion rate, and therefore could be used quantitative evaluation of cavitation erosion of material.

Chudina in 2002 has published work about noise as a cavitation indicator [27]. It was found that emitted spectra of sound give a specific response with some frequencies strongly dependent on the cavitation process. The suggested method lets to define the beginning of cavitation and set equipment for a functioning mode free of cavitation.

Some works have suggested electrochemical methods to measure cavitation erosion, evaluating combined erosion from corrosion and cavitation damage. Amann et al. [1] have developed an indirect technique to monitor and quantify cavitation erosion-corrosion of cells.

# 3. Materials and methods

## 3.1 Ultrasonic cavitation-erosion equipment

Ultrasonic cavitation-erosion equipment used in this work is based on the Fisher Scientific Sonic Dismembrator Model 500. The laboratory set includes power supply and control unit (1), cooling bath (2), sample support with immersed ultrasonic horn in noise isolation box (3). The image of used set is presented in Figure 7.


**Figure 7.** Ultrasonic cavitation-erosion equipment.

Energy transfer from electrical energy to vibration movement is performed by transducer. The transducer used in current work is Branson CR-20 with working frequency of 20 kHz. Transducer itself, creates low amplitude vibrations – to increase obtained amplitude ultrasonic horn is connected to mechanical amplifier increasing oscillation amplitude of the tip. Amplifier 1/2" Dia. Solid Exponential was used in the experiment. Connected transducer and ultrasonic horn are presented in Figure 8.

**Figure 8.** Transducer connected with the ultrasonic horn.

Amplitude of the vibratory movement is managed by the amplifier Fisher Scientific Sonic Dismembrator Model 500 presented in Figure 9.


**Figure 9.** Fisher Scientific Sonic Dismembrator Model 500.

## 3.2 Resonance frequency of the grain

Grain removal mechanism can be driven by matching of applied ultrasonic frequency and resonance frequency of one or several grains. To ensure that no resonance effect presents on working frequency, natural frequency of a single grain need to be calculated. Validation of hypothesis suggests calculation

of the resonance frequency of the grain with known size attached to the specimen's surface with the binder.

To verify this hypothesis we calculate the natural frequency of the grain attached to the specimen by specific binder. Natural frequency of oscillation system can be calculated with equation (4):

$$\upsilon = \frac{1}{2\pi}\sqrt{\frac{k}{m}}, \tag{4}$$

where $\upsilon$ is the natural frequency, k the "spring" constant and m the mass of the body.

Grain mass can be estimated with very good precision as we have well-defined size distribution and density of WC $\rho$. Grain mass calculation is performed on the average grain size of 1 micrometer.

Estimation of spring constant k, of the binder requires assumptions. We assume that ultrasonic wave loads grain on the specimen's surface, so grain are attached with binder only from one side. We use schematic (Figure 10) of a grain attached by a binder neck to the specimen's surface, so the grain itself undergoes some separation of the bulk of the specimen. Damping in the system is neglected.

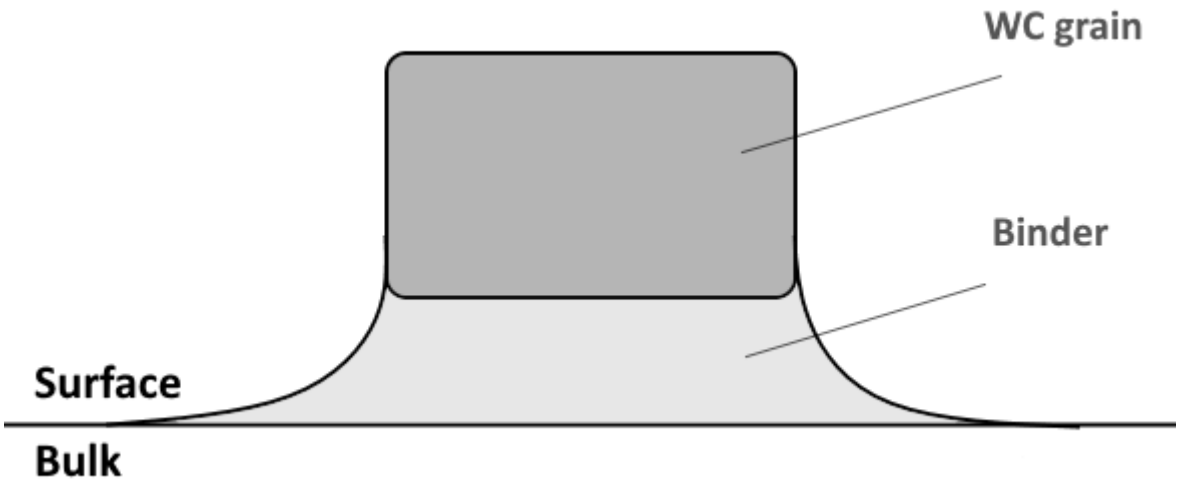


**Figure 10.** Schematic of WC grain attached to the surface with binder neck.

To calculate the spring constant, equation 5 is used, where l is the thickness of the binder neck that is estimated at 13% of WC-grain size (due to 13% binder volume content in the specimen composition), S is the cross-sectional area of the neck, taken equal to WC grain cross-section and E the Young's modulus of the binder (Nickel binder is used for calculation).

$$k = \frac{E * S}{l} \tag{5}$$

Final calculations of natural frequency is presented in the equation (6):

$$\upsilon = \frac{1}{2\pi}\sqrt{\frac{k}{m}} = \frac{1}{2\pi}\sqrt{\frac{E * S}{\rho * V * l}} = 37 * 10^{9} Hz \quad (6)$$

The driving frequency of ultrasonic equipment is 20 kHz, even with expected calculation error exceeding the obtained value by several orders of magnitude due to progressive neck cross-section decrease we obtain natural frequency exceeding driving frequency by several orders of magnitude. To conclude, the hypothesis of resonance effect within grain removal mechanism can be rejected.

## 3.3 Experimental protocol

There are seven different WC-based hardmetals we aim to analyze and compare in this work. Experimental procedure protocol have been developed to ensure similar conditions during all the experiments.

Experimental protocol covers rules of treating specimens during and after the experiments – it includes duration and number of cycles of cavitation erosion experiments, settings of ultrasonic equipment, type and temperature of used liquid, material and finishing of counterbody, etc. Work protocol also covers procedure of erosion measurements and corresponding calculations and data analysis.

Definition of cycle duration and number of cycles was taken from experiment, providing time of cavitation erosion initiation and saturation at given conditions. It was found that 24 hours cycles provide good representation of all expected cavitation erosion stages: incubation, acceleration, deceleration and terminal stages. More resistant compositions provide slower erosion development and even no significant erosion after the first cycle of work. Therefore, initially set five cycles of cavitation production are increased by additionally introduced cavitation cycles when necessary for more resistant composites.

Transducer of the cavitation erosion equipment provides stable vibration at frequency of 20 kHz – variation of the frequency is within the range 19.85 – 20.05 kHz according to the technical specification of the Digital Sonifier used. Amplifier of the horn is capable of providing the distance amplitude within the range 10.0 – 65.0 μm, in the experiment the amplifier was set for 70% power output providing amplitude 50 μm.

Several means of temperature control was used in the experiment, as continues vibratory motion inside the liquid increases its temperature due to friction over long cycles. During all the experiment,

temperature is monitored using immersed temperature sensor connected to cooling system. Cooling liquid is isolated into separate circuit – double wall vessel is used for these means. Cooling system consists of fans system and aluminum radiator. Heated water transfers the heat through the double wall vessel to cooling circuit liquid, cooling liquid is transferred to the radiator by the circuit pump and heat transferred to radiator is dissipated with air motion produced by directed fans. Applied cooling system is active once the temperature of the liquid rises over 25°C and stops once the temperature is two degrees less than the set point.

After every experimental cycle, water is changed to clean distilled water to avoid the influence of hard particles in the cavitation erosion rate.

The counterbody material was AISI 316 stainless steel. New counterbody is also used for every experimental cycle. Counterbody is securely placed on the top of the horn and cavitation occurs within the volume of liquid in the close proximity to counterbody surface. Diameter of the counterbody is 15.9 mm what corresponds to active area of cavitation erosion occurrence (Figure 11). Before applying the counterbody, the surface is mirror-polished with SiC polishing abrasive paper with: grit 80, 220, 360, 800, 1000, 2000, finishing with diamond paste 3 μm.

Specimen placed into the support and fixed by 1.0 mm distance from the ultrasonic horn with counter-body using plates metric filler. The distance is chosen using experience of previous researchers and adjusted by preliminary test to obtain the highest erosion rate.

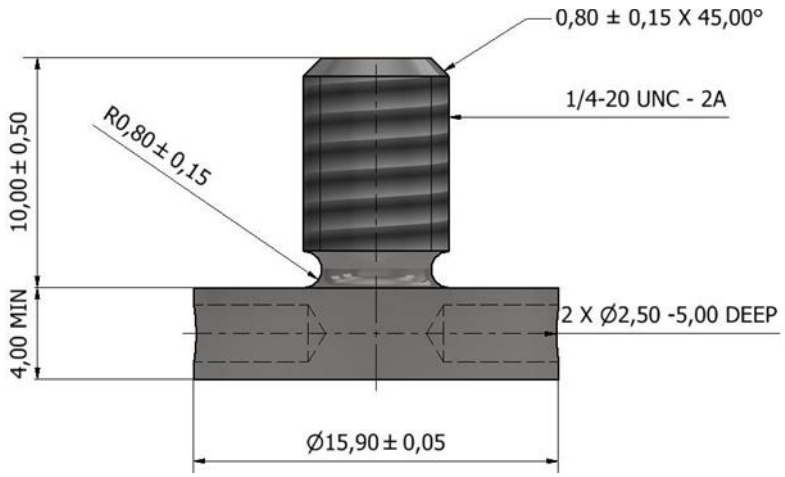


**Figure 11.** Dimensions of the counterbody.

Before the specimen is proceeded for measurements it is cleaned using ultrasonic bath to ensure that all the detached particles are removed from the surface before profilometric measurements. Specimen is placed into ultrasonic bath for cleaning during 30 minutes where the liquid used for cleaning is acetone.

## 3.4 Specimens characterization

Tungsten carbide composites are known due to their dense microstructure, low porosity and high hardness keeping significant fracture toughness. Tungsten carbide specimens with different binders have been received from DURIT Hartmetall company. The chemical composition of the different WC-composites are provided in the Table 1.

**Table 1.** Nominal composition of the prepared hardmetal grades.

| Composition | Composition (wt.%) | | | | | Binders composition (wt.%) | | | | Composition (vol.%) | |
|---|---|---|---|---|---|---|---|---|---|---|---|
| | WC | Co | Ni | $Cr_3C_2$ | $Mo_2C$ | Co | Ni | Cr | Mo | WC | Binder |
| WC-Co | 92.0 | 8.0 | - | - | - | 100.0 | - | - | - | 86.8 | 13.2 |
| WC-Ni | 92.0 | - | 8.0 | - | - | - | 100.0 | - | - | 86.8 | 13.2 |
| WC-CoNi | 92.0 | 5.5 | 2.5 | - | - | 68.8 | 31.2 | - | - | 86.8 | 13.2 |
| WC-CoCr | 92.0 | 7.2 | - | 0.8 | - | 91.2 | - | 8.8 | - | 86.7 | 13.0 |
| WC-NiCr | 91.2 | - | 8.0 | 0.8 | - | - | 92.0 | 8.0 | - | 85.4 | 14.6 |
| WC-CoNiCr | 94.2 | 3.5 | 1.5 | 0.8 | - | 61.5 | 26.3 | 12.2 | - | 90.2 | 9.8 |
| WC-NiCrMo | 90.6 | - | 8.0 | 0.8 | 0.6 | - | 86.4 | 7.5 | 6.1 | 84.7 | 15.3 |

Initial surface roughness parameters have been measured with profilometer Mitutoyo SJ-500. For each sample three measurement have been performed, based on the measurements average values and standard deviations have been calculated. Measured surface roughness parameters with corresponding standard deviations are presented in the Table 2.

**Table 2.** Surface roughness parameters for the different hardmetal grades.

| Code | Composition | $R_a$ (μm) | $R_q$ (μm) | $S_k$ | $K_u$ |
|---|---|---|---|---|---|
| C1 | WC-Co | 0.073 ± 0.006 | 0.094 ± 0.003 | -0.045 ± 0.011 | 3.332 ± 1.012 |
| C2 | WC-Ni | 0.076 ± 0.01 | 0.095 ± 0.012 | -0.014 ± 0.054 | 2.794 ± 0.155 |
| C3 | WC-CoNi | 0.068 ± 0.019 | 0.085 ± 0.024 | -0.002 ± 0.035 | 2.855 ± 0.001 |
| C4 | WC-CoCr | 0.077 ± 0.008 | 0.097 ± 0.01 | -0.035 ± 0.002 | 2.969 ± 0.082 |
| C5 | WC-NiCr | 0.061 ± 0.013 | 0.076 ± 0.016 | -0.037 ± 0.034 | 2.95 ± 0.293 |
| C6 | WC-CoNiCr | 0.065 ± 0.009 | 0.081 ± 0.011 | -0.025 ± 0.008 | 2.884 ± 0.077 |
| C7 | WC-NiCrMo | 0.066 ± 0.004 | 0.082 ± 0.004 | -0.005 ± 0.008 | 2.893 ± 0.152 |

The mechanical characterization for the different composites are collected in the Table 3 including density, elastic modulus, hardness and fracture toughness. Density and elastic modulus values for the different composites were determined previously at DURIT Hartmetall. The density of composites with different binders is found within the range 14.55 – 14.82 g/cm$^3$. Narrow 2 % difference range of density values originates from high percentage of base WC in the composition of hardmetals, fraction of binders within each composition is within 8-10%. Highest values of density and elastic modulus are corresponded to specimen WC-CoNiCr providing highest fraction of WC grains 94.2% of total mass as can be seen in Table 1.

Porosity of the WC-based composites have been investigated according to ISO 4499-4:2016 standard within ABC-classification – received microstructure of the specimen is A00B00C00 according to the ISO [28]. Excellent porosity properties are conditioned by both manufacturing method and grain size used. WC grain size in the range 0.4 – 3.17 μm were used to produce the composites, using sintering method. Particles distribution used for specimen sintering is provided on the Figure 12. During the sintering process, particles are melted together, and shrinkage of pores volume can be observed.

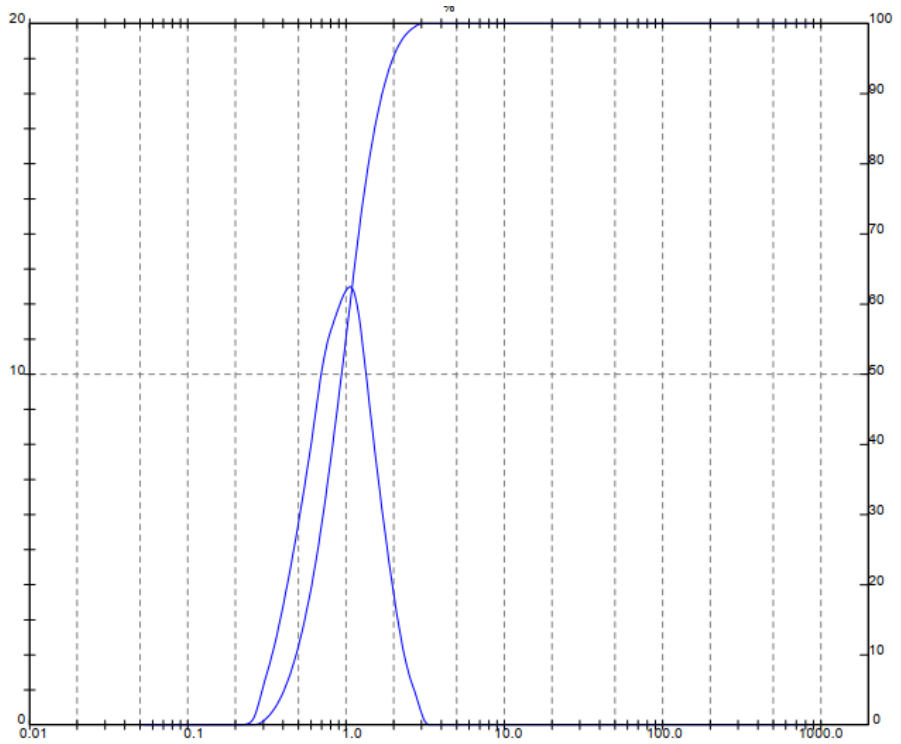


**Figure 12.** WC particle distribution (source: DURIT hartmetall).

Mechanical properties of provided specimens are provided in Table 3.

**Table 3.** Mechanical properties for the different hardmetal grades.

| Code | Composition | Dens. ($g/cm^3$) | E (GPa) | $HV_{30}$ ($kgf/mm^2$) | $K_{IC}$ ($MPa.m^{1/2}$) |
|---|---|---|---|---|---|
| C1 | WC-Co | 14.72 | 512 | 1432±23 | 10±.03 |
| C2 | WC-Ni | 14.69 | 522 | 1374±17 | 9.7±1.0 |
| C3 | WC-CoNi | 14.62 | 520 | 1408±2 | 13.3±0.9 |
| C4 | WC-CoCr | 14.64 | 526 | 1621±21 | 9.2±0.1 |
| C5 | WC-NiCr | 14.58 | 484 | 1442±19 | 9.9±1.2 |
| C6 | WC-CoNiCr | 14.82 | 560 | 1810±51 | 9.2±0.4 |
| C7 | WC-NiCrMo | 14.55 | 519 | 1488±8 | 10.2±0.8 |

Hardness and fracture toughness have been measured under 30 kg applied load ($HV_{30}$). Each value of hardness and fracture toughness is obtained from averaging results of the set of five different measurements. Hardness is calculated in accordance with Vickers test and fracture toughness is calculated using the Palmqvist method. Corresponding equations are provided under Equation 1 and Equation 3, respectively. During each experiment diagonals of square indentation produced by 136-

degree diamond pyramid are measured, values are used to calculate hardness. Lengths of fracture cracks in the corners of square indentation are measured during each experiment to calculate the fracture toughness for the different specimens. An example of square indentation and performed measurements are presented in Figure 13.

$$HV = \frac{F}{A}, \tag{1}$$

where F is applied force (kgf) and A is indentation area ($mm^2$).

The area of indentation is calculated by Equation 2:

$$A = \frac{d^2}{2\sin(136°/2)}, \tag{2}$$

where d is the average of two measured diagonals of indentation (mm).

To calculate fracture toughness the following equation is used:

$$KIC = 0.0028\sqrt{HV * \frac{P}{T}}, \tag{3}$$

where HV is measured Vickers hardness, P is applied load in N, T is total crack length (mm).

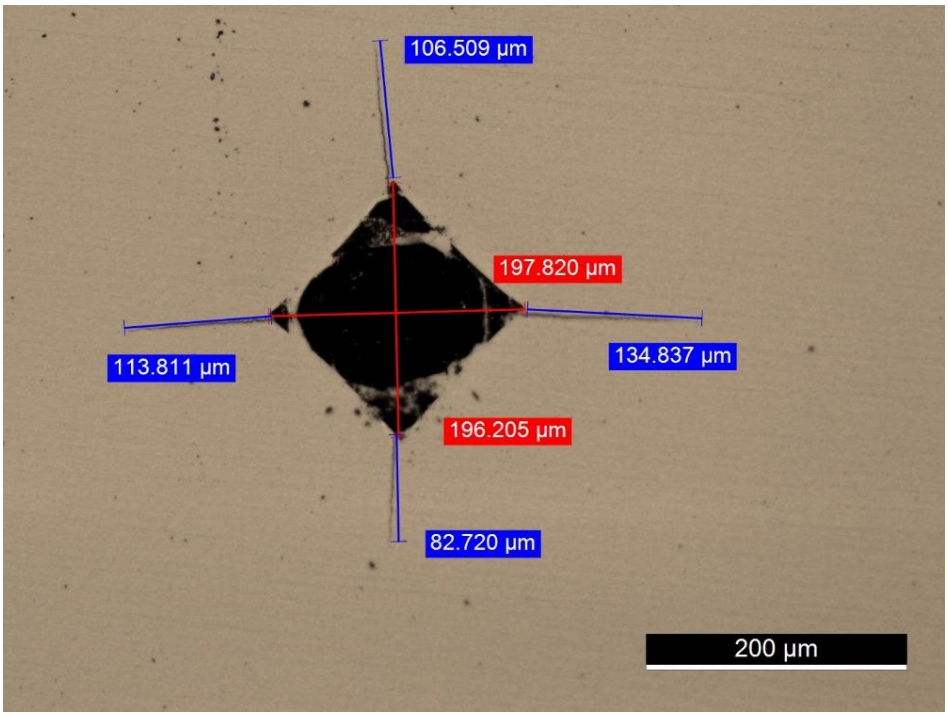


**Figure 13.** Square indentation of 136 degree pyramid with corresponding measurements.

# 4. Results and discussion

Seven different specimens of WC-based composites with different binders have been exposed to at least five cycles of cavitation-erosion, 24 hours each. In the present chapter, the results of the wear analysis of the specimens are presented.

## 4.1 3D laser profilometer measurements

3D laser profilometer Rodenstock RM600-S have been used to obtain 3D topography of eroded surfaces. 3D representation of measured results for the WC-Co specimen surface, after 24 hours of cavitation, is presented in the Figure 14. It is possible to observe that a circular hole was produced in the center of the specimen with the depth of approximately 50 μm.

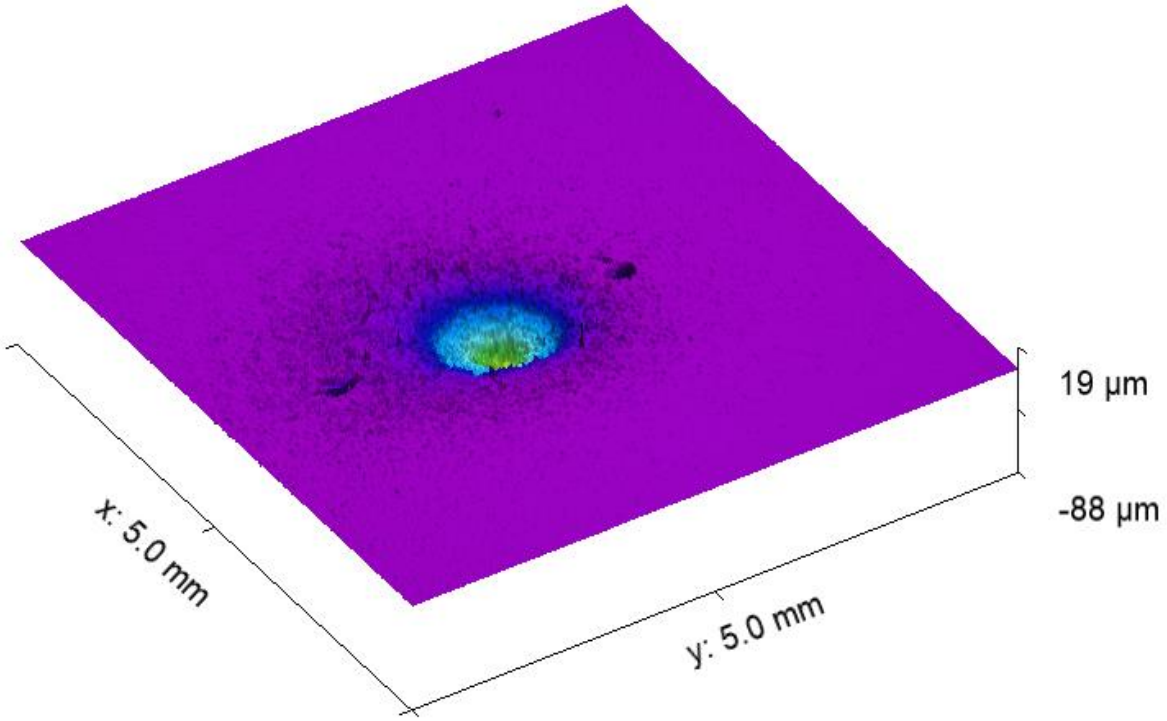


**Figure 14.** 3D profile from the surface of WC-Co, after 24 hours of cavitation-erosion cycle.

Data of 3D surface topology is collected during all cavitation-erosion cycles and 2D central profiles are extracted for measurements and relative comparison. Figure 15 presents results of WC-Co 2D profiles extracted during 5 cycles of cavitation erosion (5 x 24 h = 120 h). Data provides clear representation of profile evolution. It is possible to observe that the depth and diameter of the hole increases, in a general way, with the number of cycles.

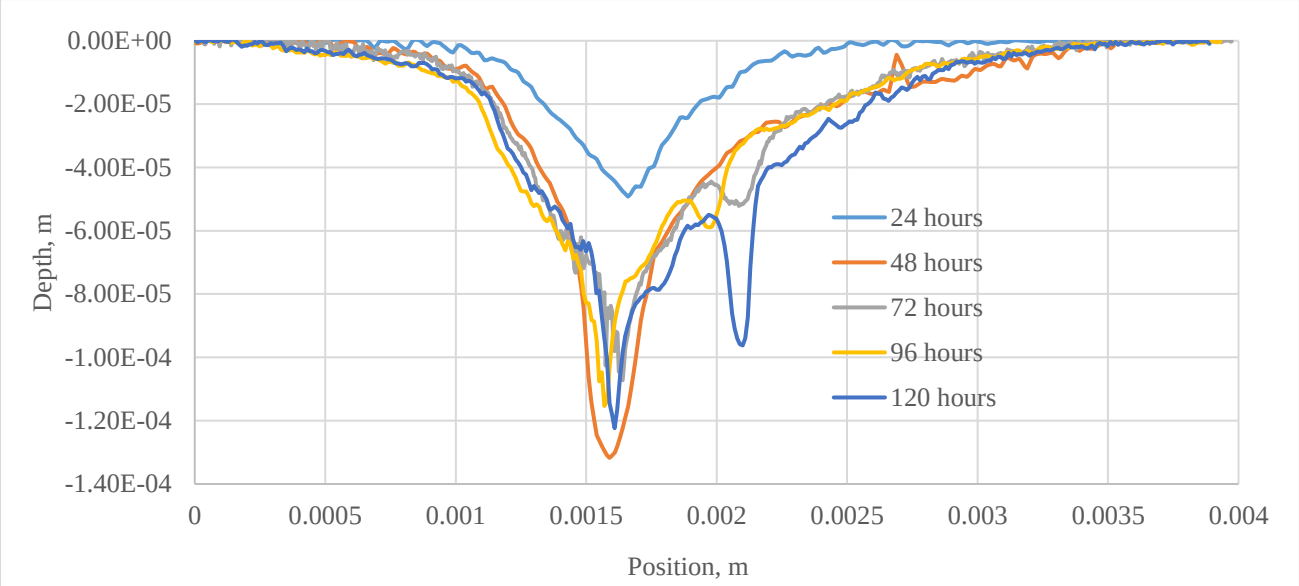


**Figure 15.** Evolution of 2D profile of WC-Co.

Erosion volume have been calculated after integrated the 3D erosion profiles and data have been collected in a form of volume loss evolution over time for all the specimens. Calculation results are presented in the Figure 16. In Figure 16-a data of all the specimen is presented and is possible to see that WC-Co specimen volume loss is one order of magnitude higher than the volume loss of the others specimens. So for better comparison, on Figure 16-b, the same data with WC-Co excluded is presented.

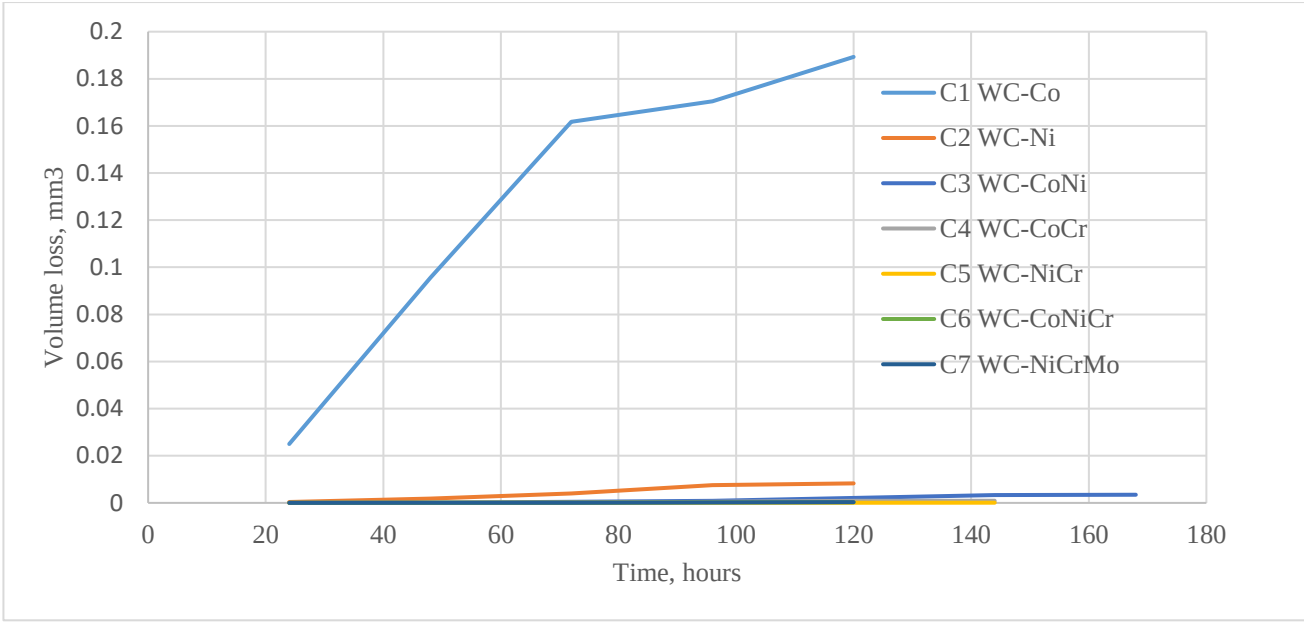


(a)

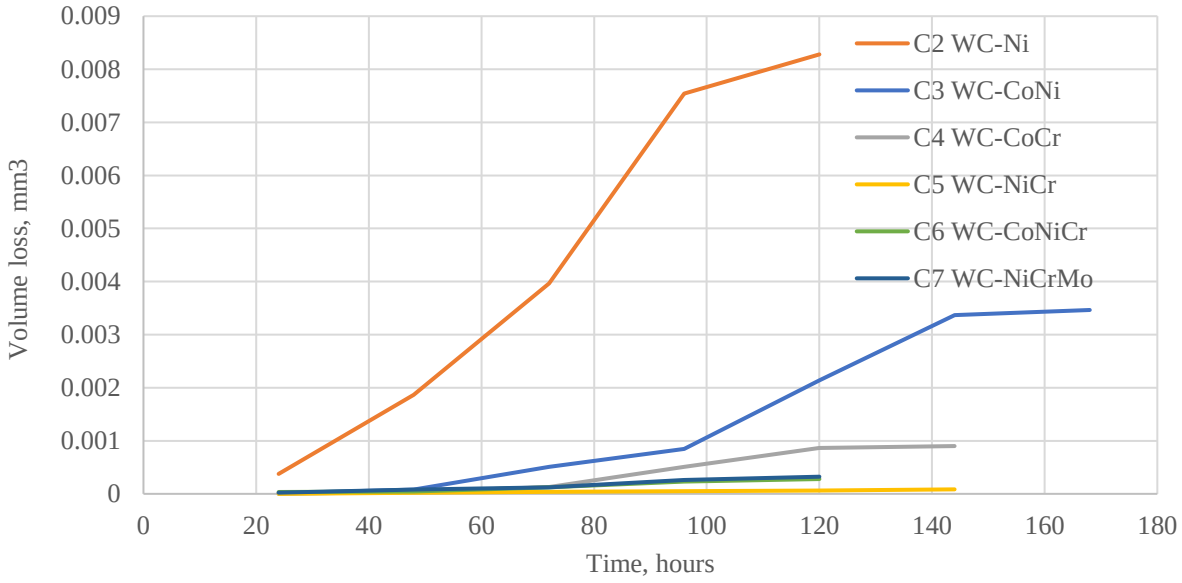


(b)

**Figure 16.** Evolution of volume loss: a) all specimens: b) WC-Co excluded.

From Figure 16-b we can see that the specimen that contains NiCr binder provided the best cavitation erosion resistance following by the specimens containing CoNiCr, NiCrMo, CoCr, CoNi, Ni, and Co binder showing the weakest performance, as revealed in Figure 16-a (light blue color). It is an important sign, that binders with Chromium in his composition provided the best wear performance over all analyzed binders, while Cobalt binder and its compositions provided the weakest wear performance.

Results shown, also correlate in great extend with the hardness measurements performed before the cavitation-erosion experiments. As shown in Table 3, it was determined that composites with chromium-based binders have higher hardness in comparison with cobalt-based binders. It is then possible to conclude that higher hardness means higher cavitation-erosion resistance.

One of used approaches for erosion rate estimation is presented in Figure 17. Every measurement stage erosion rate calculated as volume loss difference divided by the cavitation erosion time in hours. This approach allows to see local change of erosion rate on every stage of measurements. Due to higher volume loss rates of WC-Co specimen, just as it happened for the volume loss, Figure 17-b presents also results of volume loss excluding WC-Co results for better comparison.

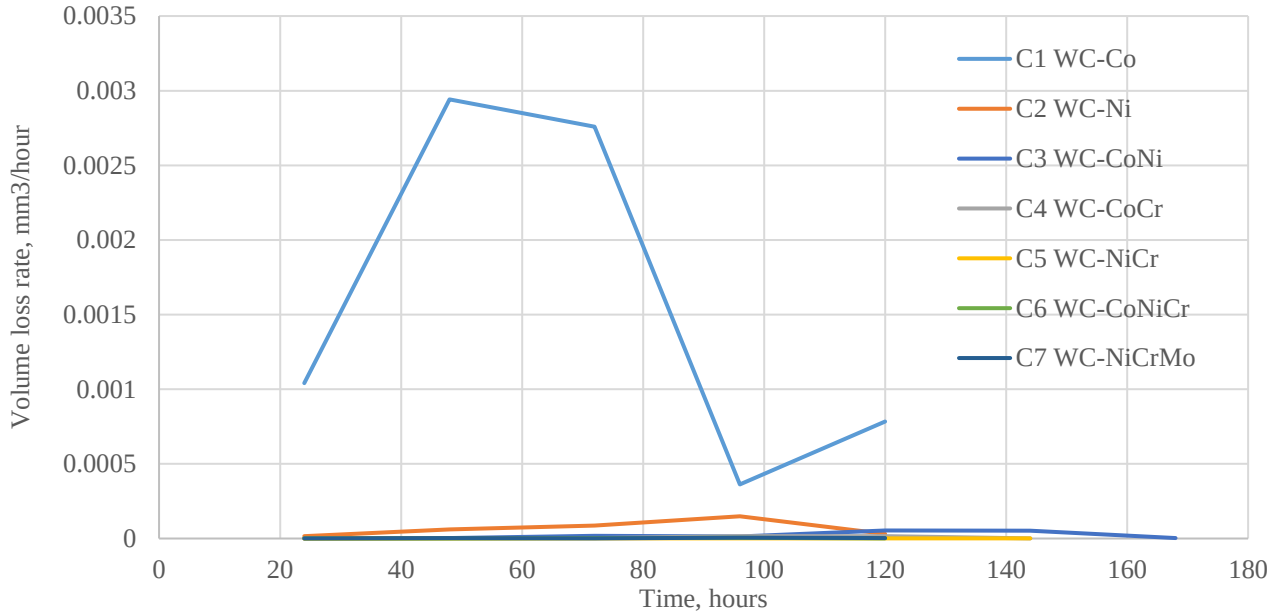


(a)

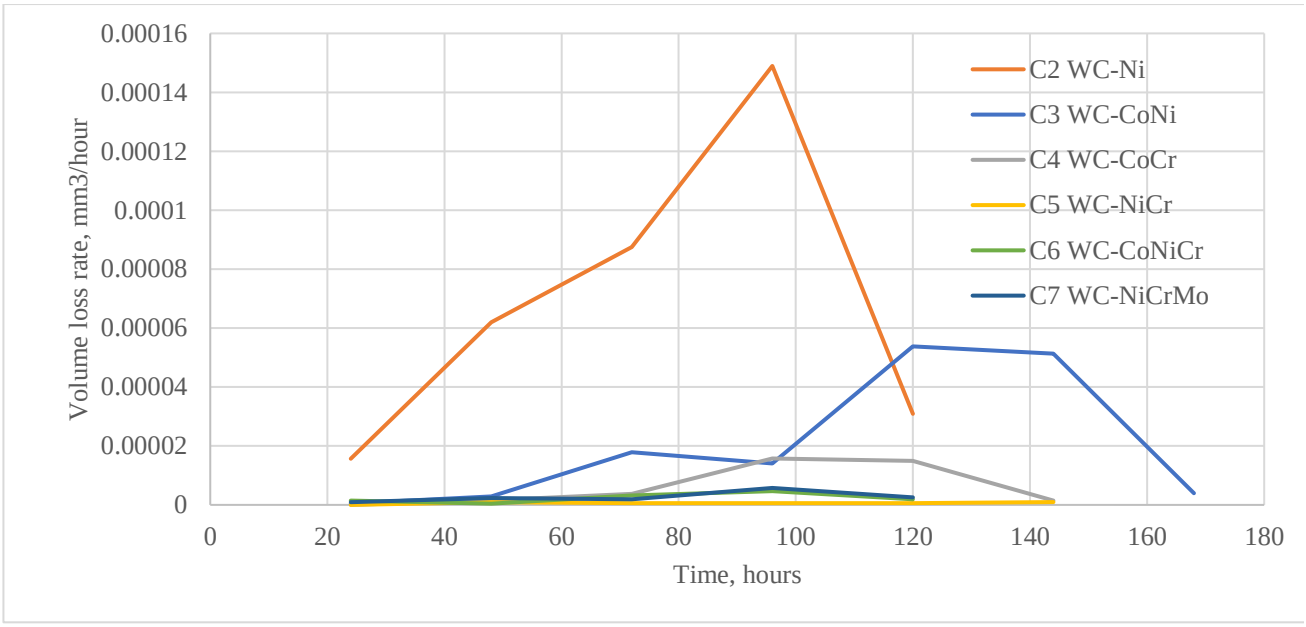


(b)

**Figure 17.** Evolution of volume loss rate: a) all specimens; b) WC-Co excluded.

Volume loss rate graphs presented in the Figure 17 demonstrates presence of several theoretically expected cavitation-erosion stages. Usually, cavitation-erosion is descreibed within 4 main stages: incubation stage, accelerating stage, decelerating stage and terminal stage. Bell-shaped form of presented graphs indicates clearly accelerating and decelerating stages of cavitation erosion.

Figures 18-24 indicate different paths of volume loss and volume loss rates. By analysing the figures, it can be seen that every specimen shows accelerating and decelerating stages of erosion rate. However, it is possible to observe different times that is required to arrive to volume loss rate picks for different binders, representing different time required for incubation stage, different amount of time and energy to complete acelerating and decelerating stages.

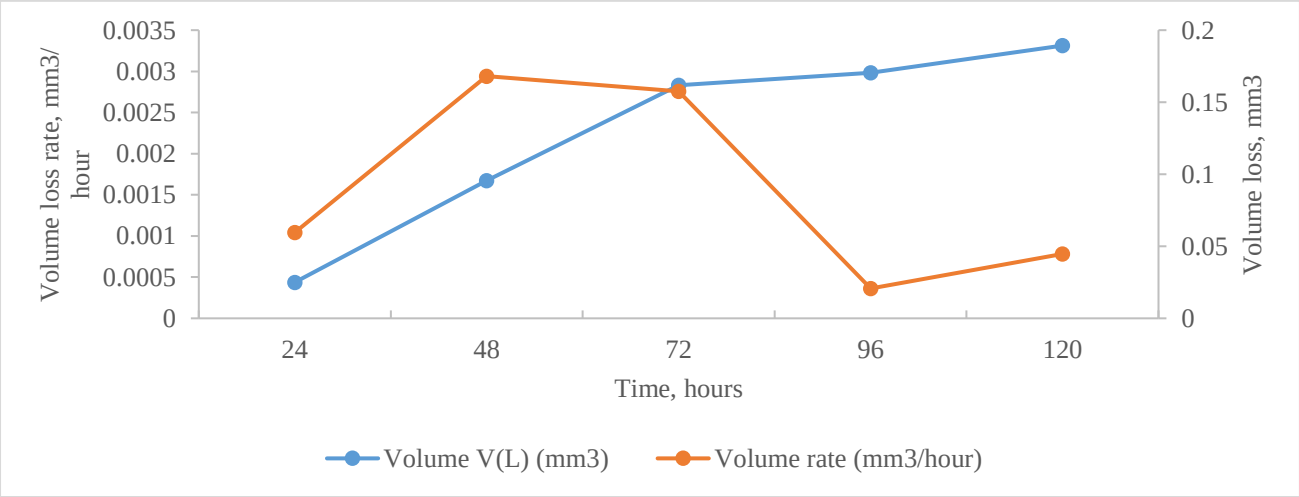


**Figure 18.** Evolution of volume loss and volume loss rate for the WC-Co specimen.

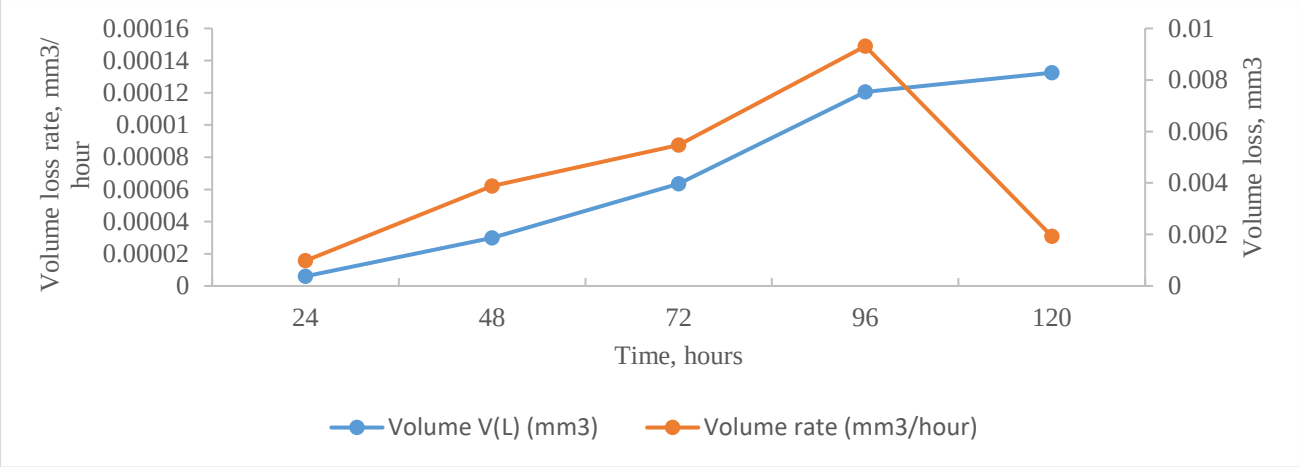


**Figure 19.** Evolution of volume loss and volume loss rate for the WC-Ni specimen.

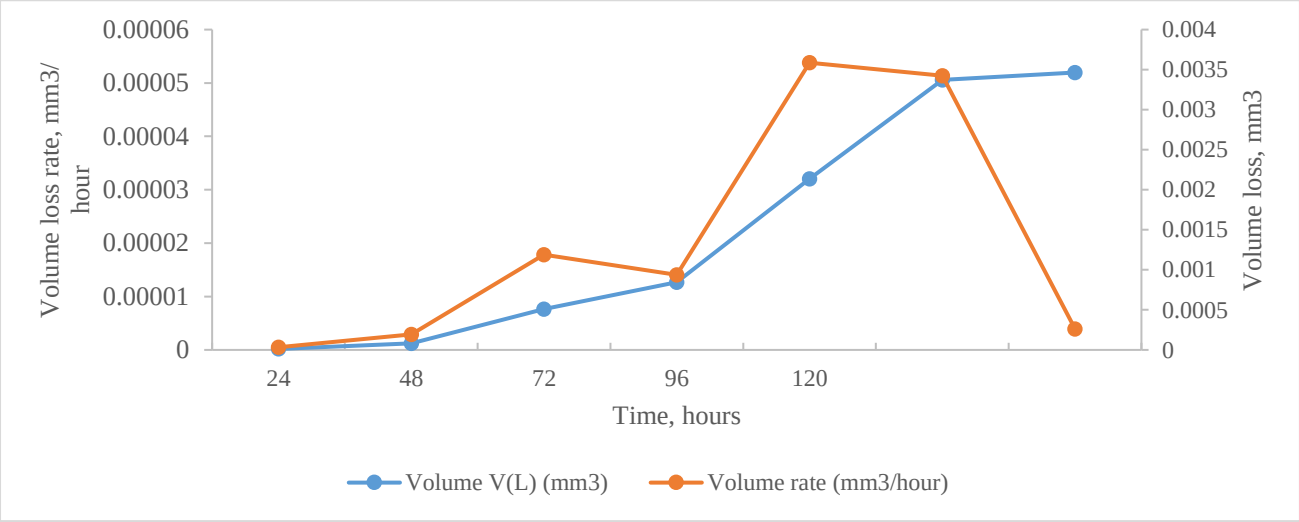


**Figure 20.** Evolution of volume loss and volume loss rate for the WC-CoNi specimen.

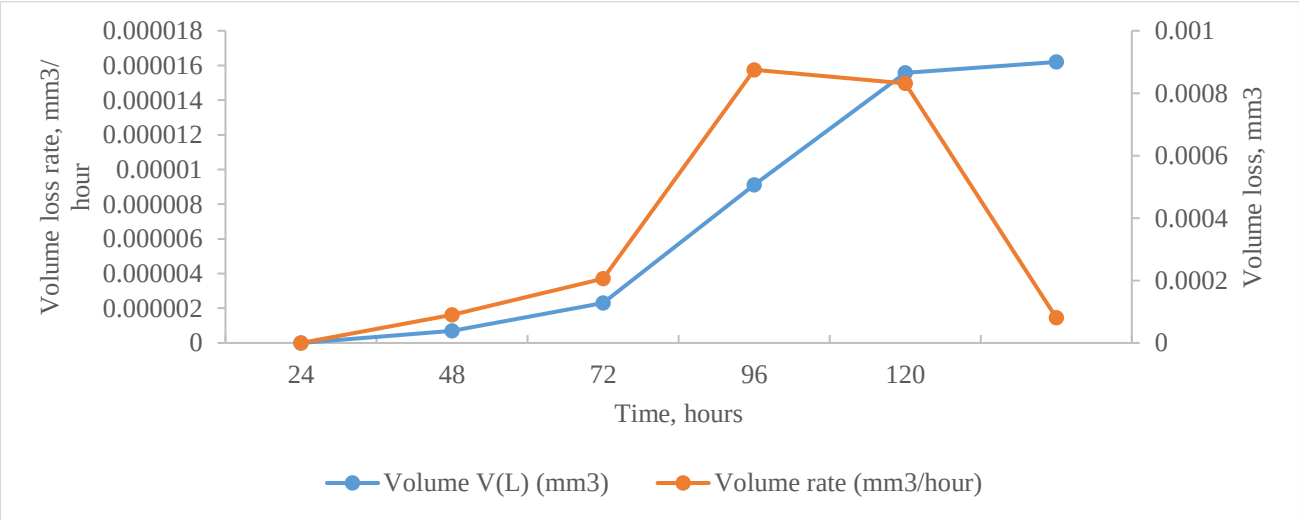


**Figure 21.** Evolution of volume loss and volume loss rate for the WC-CoCr specimen.

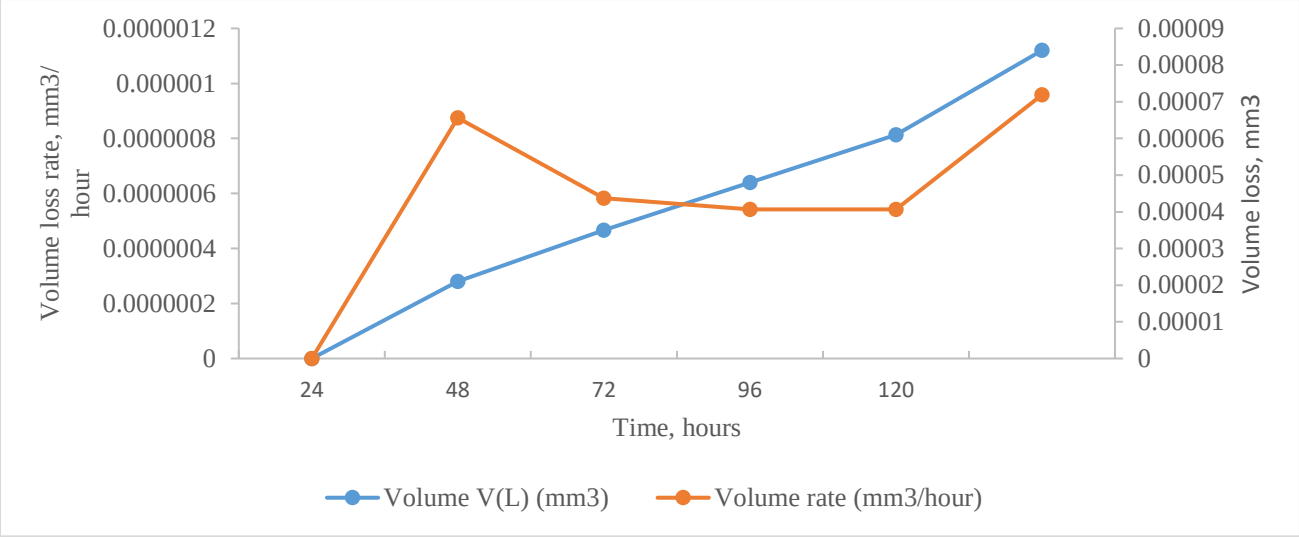


**Figure 22.** Evolution of volume loss and volume loss rate for the WC-NiCr specimen.

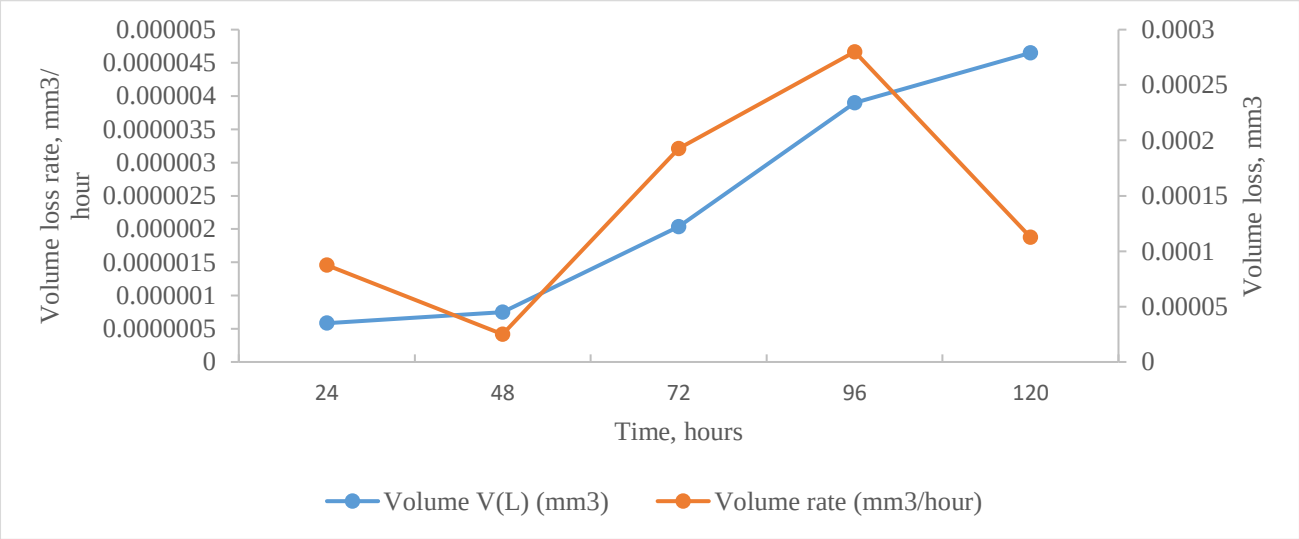


**Figure 23.** Evolution of volume loss and volume loss rate for the WC-CoNiCr specimen.

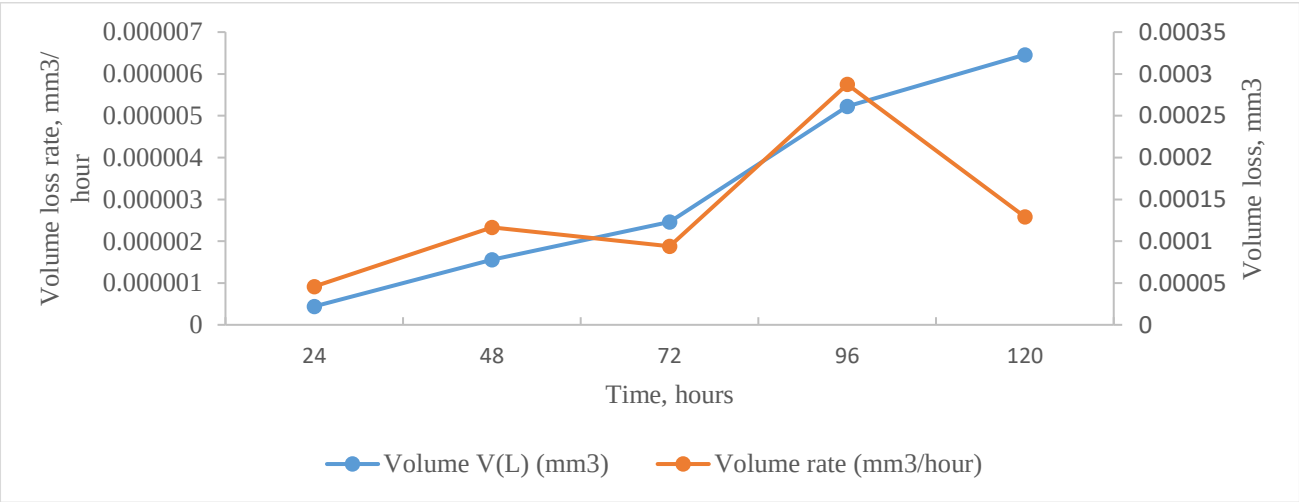


**Figure 24.** Evolution of volume loss and volume loss rate for the WC-NiCrMo specimen.

Two out of four cavitation erosion stages have been observed using volume loss rate curves. Observation of first incubation stages would require selection of a smaller time step at the beginning of the cavitation erosion experiment. Terminal stage observation would require to add several cavitation erosion cycles and increase duration of the experiment.

We can observe that WC-Co, WC-CoNi, WC-CoCr and WC-NiCoMo volume loss graphs (Figure 18, 20, 21, 24) have presented two cavitation erosion stages with different erosion rates, WC-Ni, WC-NiCr and WC-CoNiCr (Figure 19, 22 and 23) have presented almost linear progression of volume loss. This observation suggests us use another approach for cavitation erosion volume loss rate, which is presented on the Figures 25-31.

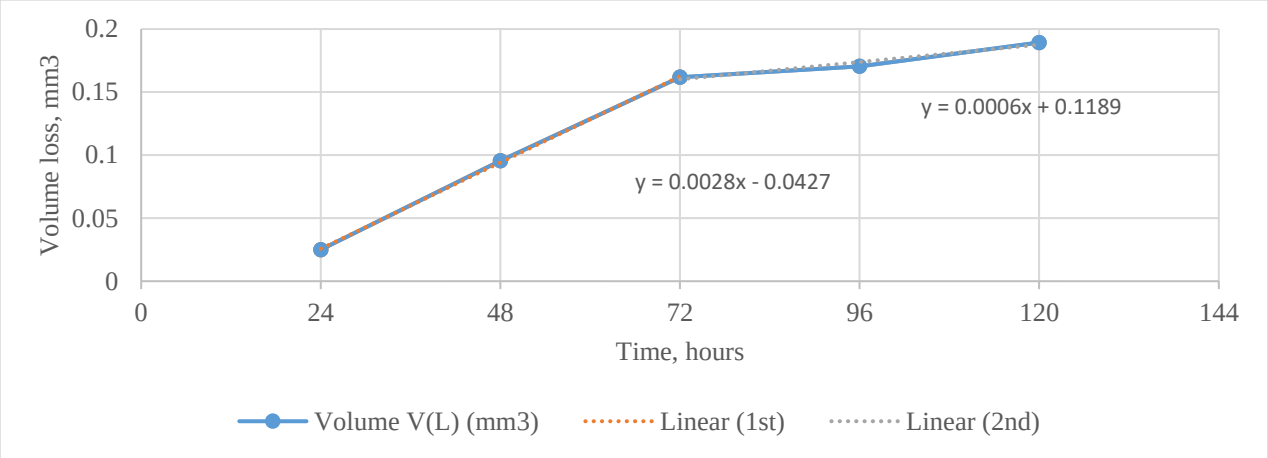


**Figure 25.** Volume loss chart and cavitation erosion rate calculation WC-Co

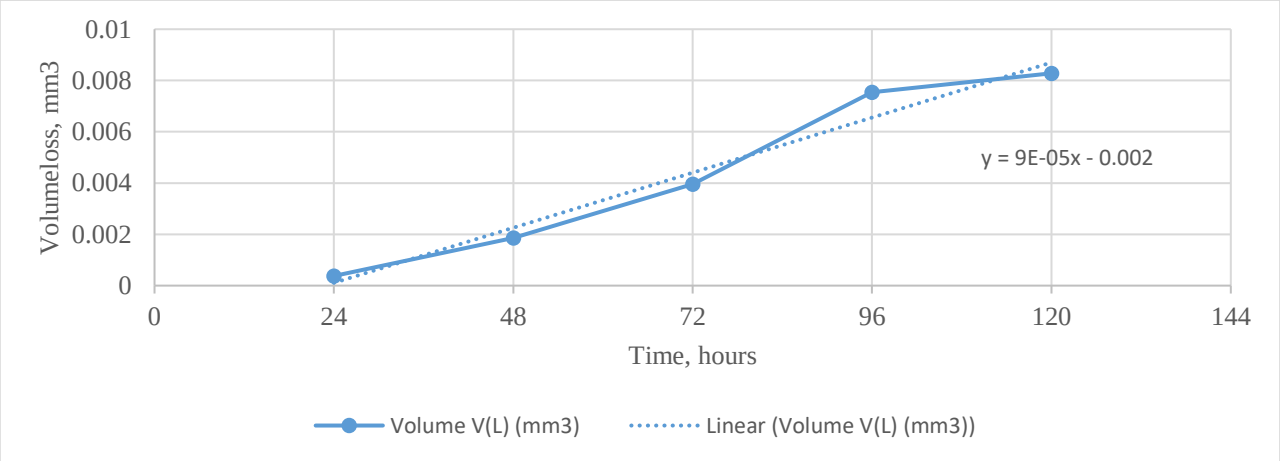


**Figure 26.** Volume loss chart and cavitation erosion rate calculation WC-Ni

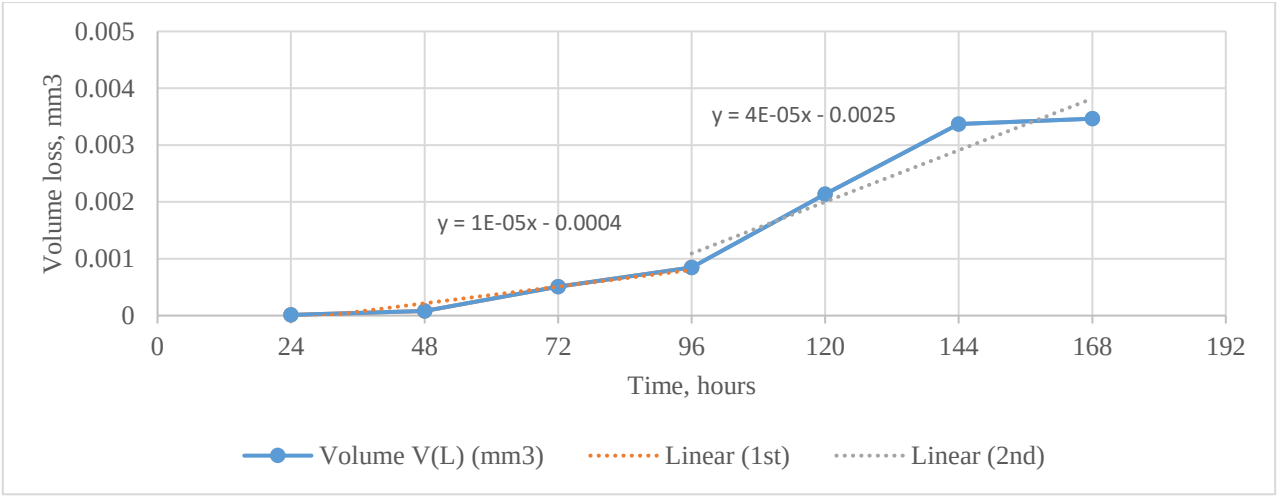


**Figure 27.** Volume loss chart and cavitation erosion rate calculation WC-CoNi

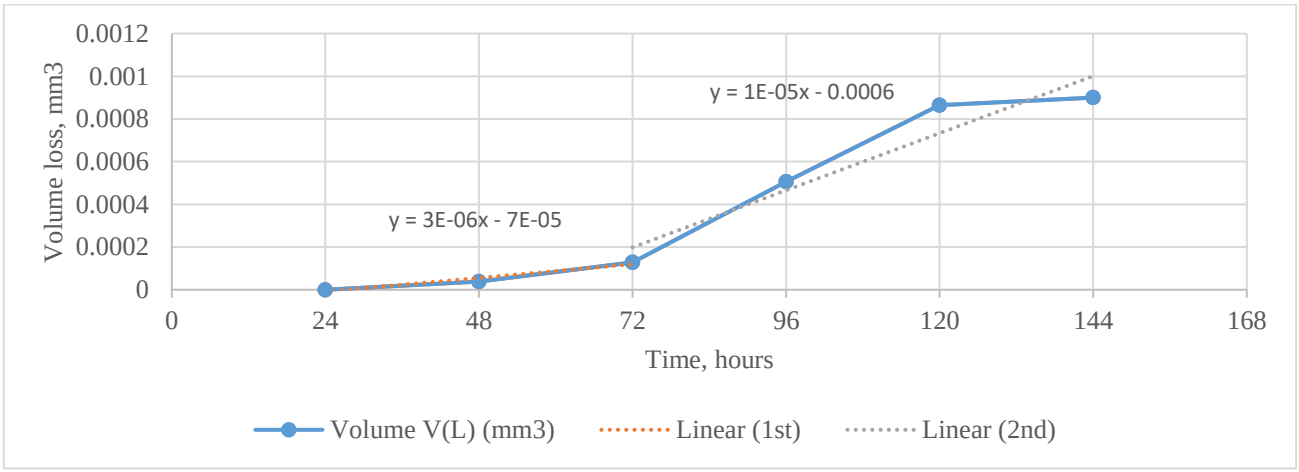


**Figure 28.** Volume loss chart and cavitation erosion rate calculation WC-CoCr

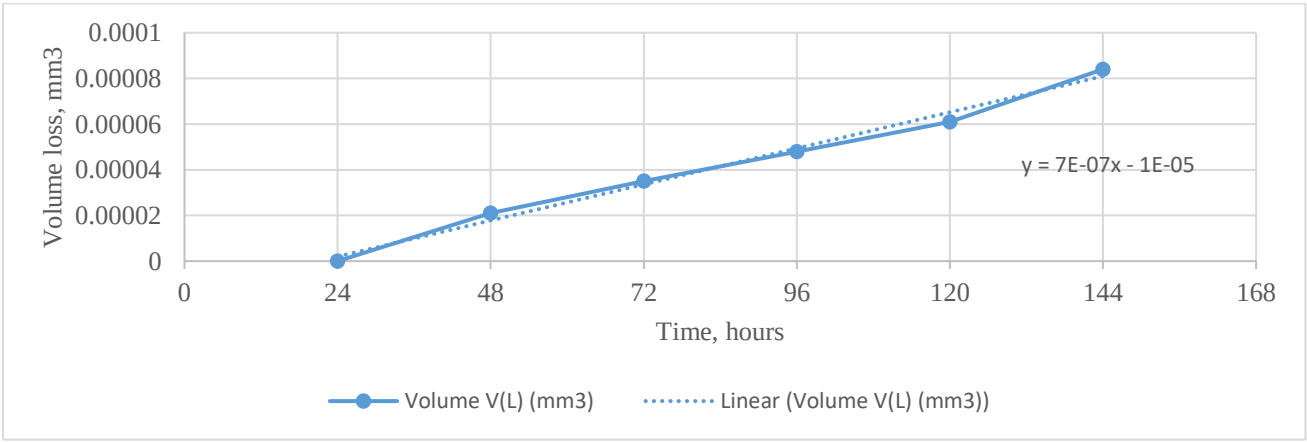


**Figure 29.** Volume loss chart and cavitation erosion rate calculation WC-NiCo

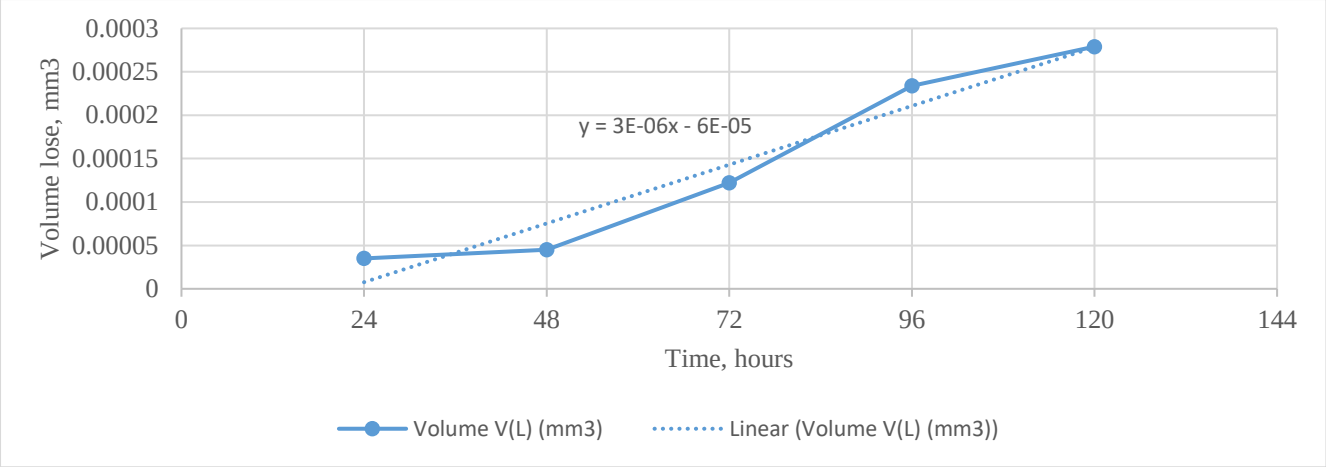


**Figure 30.** Volume loss chart and cavitation erosion rate calculation WC-CoNiCr

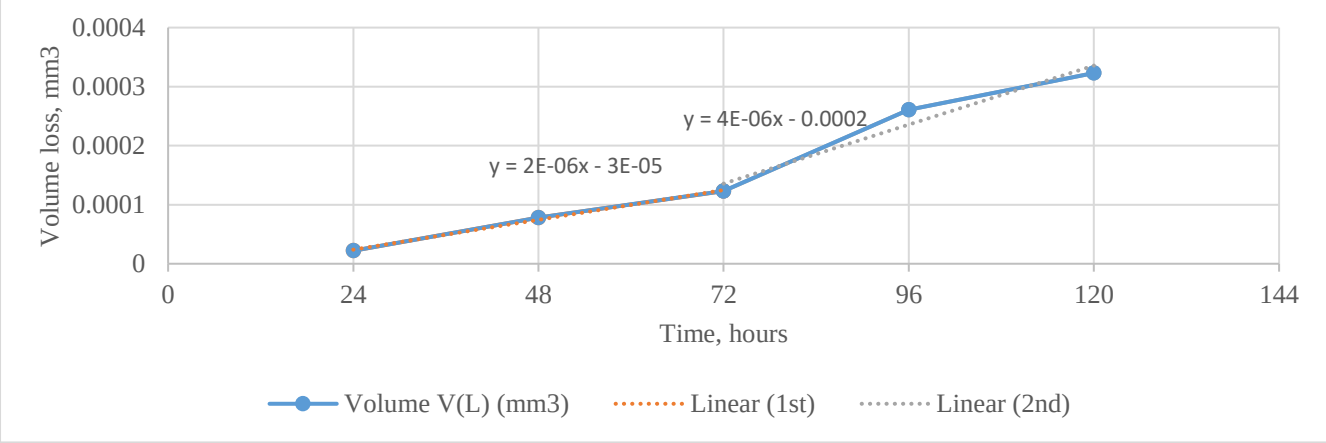


**Figure 31**. Volume loss chart and cavitation erosion rate calculation WC-NiCrMo

Volume loss graphs have divided into stages of nearly linear grows and erosion rates are calculated separatly on the each stage. Trendlines are presented on the Figures 25-31 and the results of volume loss rate calculations are collected in the Table 4. Maximum erosion rate values are used to compare different binders, this results provide clear quantification of comparison of the binders performance.

**Table 4.** Erosion rates of the different specimens at the different stages (mm3/hour)

| | **WC-Co** | **WC-Ni** | **WC-CoNi** | **WC-CoCr** | **WC-NiCr** | **WC-CoNiCr** | **WC-NiCrMo** |
|---|---|---|---|---|---|---|---|
| **Erosion rate 1st stage** | 0.00282 | 8.9e-5 | 1.22e-5 | 0.26e-5 | 0.66e-6 | 2.82e-6 | 2.11e-6 |
| **Erosion rate 2nd stage** | 0.000572 | | 3.75e-5 | 1.11e-5 | | | 4.17e-6 |
| **Max. erosion rate** | 0.00282 | 8.9e-5 | 8.9e-5 | 1.11e-5 | 0.66e-6 | 2.82e-6 | 4.17e-6 |

## 4.2 Grain size estimation using FFT

Fast Fourier Transform (FFT) is used to convert received signal from it's original domain to a representation in the frequency domain and vice versa [29]. Application of FFT on the measured 2D profiles, transfers the topography of the surface into the frequency of surface characteristic features: grains, pits and defects. The method provides opportunity to look for features in specific size ranges providing the main frequency of the feature occurrence.

Profilometer Mitutoyo SJ-500 is used to obtain 2D profiles from the eroded area. Unprotected WC grains after binder removal are creating surface irregularities. FFT can be used in order to extract the size of the irregularities and corresponding frequencies. Grain size is expected to be a close match with particles' size used in the process. Most of the particles have a size of around 1 μm, the same corresponding resolution of the profilometer that was used to collect data on all the features. Step size/resolution of 0.5 μm was used to obtain 2D profile data.

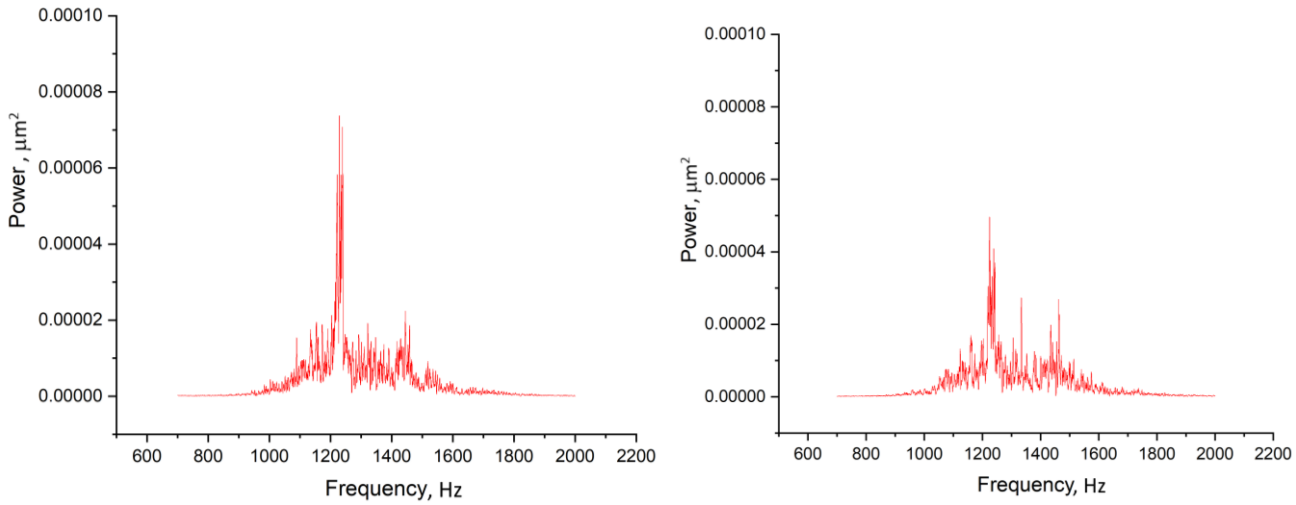


**Figure 32.** FFT of WC-Cospecimen profile: a) before cavitation-erosion; b) after cavitation-erosion.

From Figure 25 we can find out that FFT picks corresponds to the frequency ~ 1200 Hz and the overall range is found between 1000 and 1800 Hz. Equation (7) provides the way to connect frequency with surface feature size – grain size.

$$Grain\ size = \frac{1000}{\nu} = \frac{1000}{1200} = 0.83\ \mu m \qquad (7)$$

The grain was defined in indirect way using FFT where grain size is estimated to be equal 0.83 $\mu m$. Using this method grain size is expected to be underestimated as biggest grain dimension is hidden from the measurement under the surface and only part of the grain is reachable for direct measurement.

Comparing FFT analysis results before cavitation and after cavitation it is possible to observe matching ranges and frequency picks, what let us suggest that even mirror polished surface can reveal grain size information.

## 4.3 SEM analysis

Scanning electron microscopy (SEM) have been used to observe specimens' surfaces with higher magnification. Energy dispersive X-Ray spectroscopy (EDS) have been applied to obtain compositional analysis of the specimens. Eroded zones of the surface of WC-Co specimen, where SEM analysis have been performed is showed in Figure 26. The initial mirror-polished surface is completely undetectable at the eroded zones.

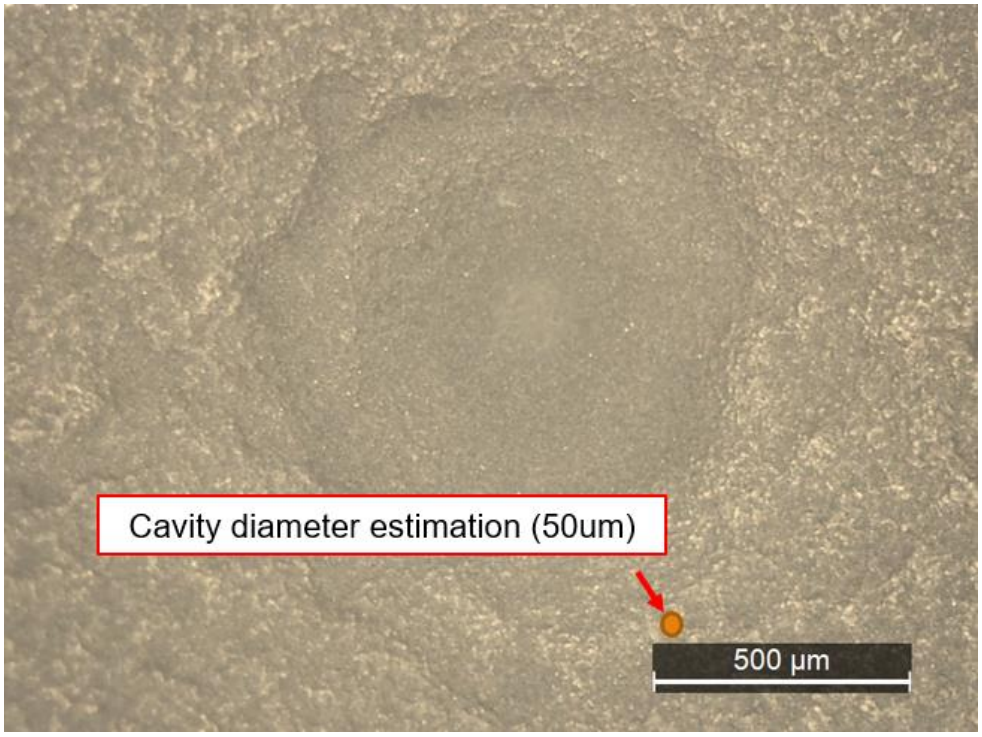


**Figure 33.** Cavitation-erosion pit on the surface of WC-Co specimen.

Figure 27 provides x7000 magnification of the WC-Co surface. It is possible to observe separate grains on the surface, most of the grains are visible as "naked" grains without any binder. However, some spots with binder presence is still observable as marked by a red circle in Figure 27.

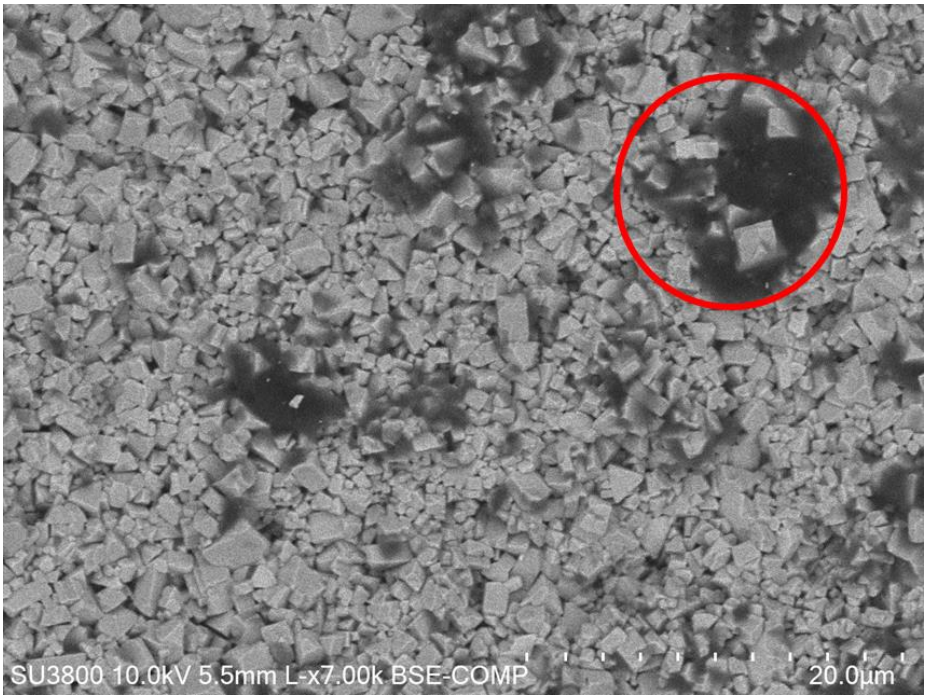


**Figure 34.** SEM image of eroded area of WC-Co specimen.

All the WC grains observed under high magnification are undamaged, clear grain edges are visible. Most of pey grains are not covered with any binder, which suggests that cavitation-erosion mechanism involves soft binder removal at the first place, what leads to complete grains detachment after it.

Hardness is one of the most important mechanical properties that must be considered to predict severe cavitation-erosion. WC grains are ceramic grains with much higher hardness value than all metal binders used in the present research investigation. It suggests lower cavitation erosion-resistance of binder and its prioritised removal over hard WC grains.

## 4.4 EDS compositional analysis

EDS analysis have been performed on the eroded area of the specimens to evaluate compositional changes on the surfaces. In Figure 28, representation of the line scan performed over the eroded area of the WC-CoCr specimen is presented (yellow line). The evolution of the chemical composition over the line scan and the EDS spectra can be seen in the Figure 29.

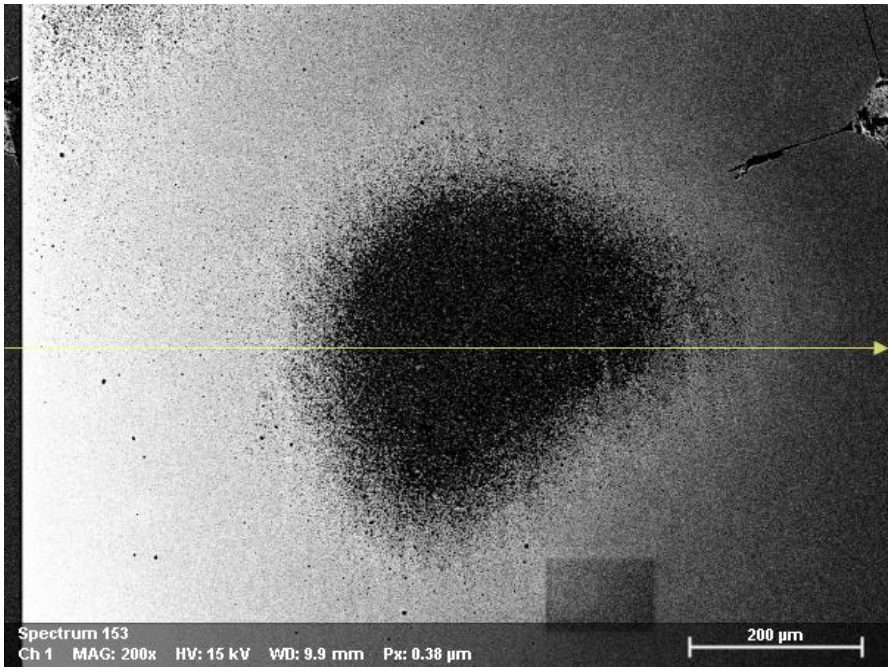


**Figure 35.** EDS line scan over WC-CoCr eroded surface.

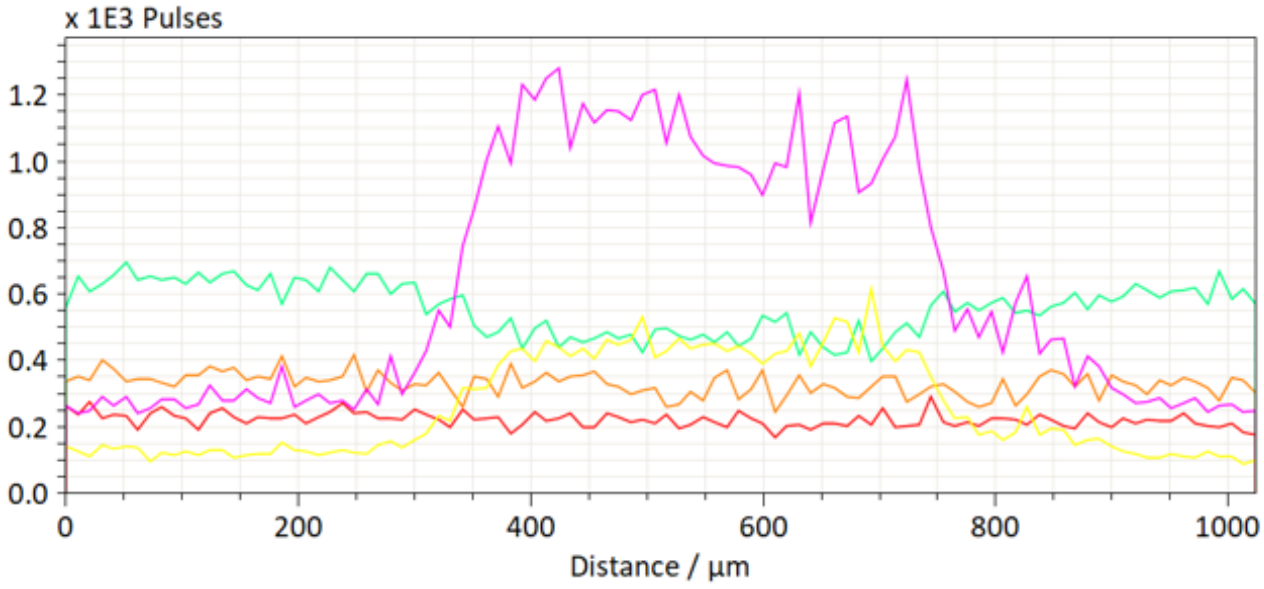


(a)

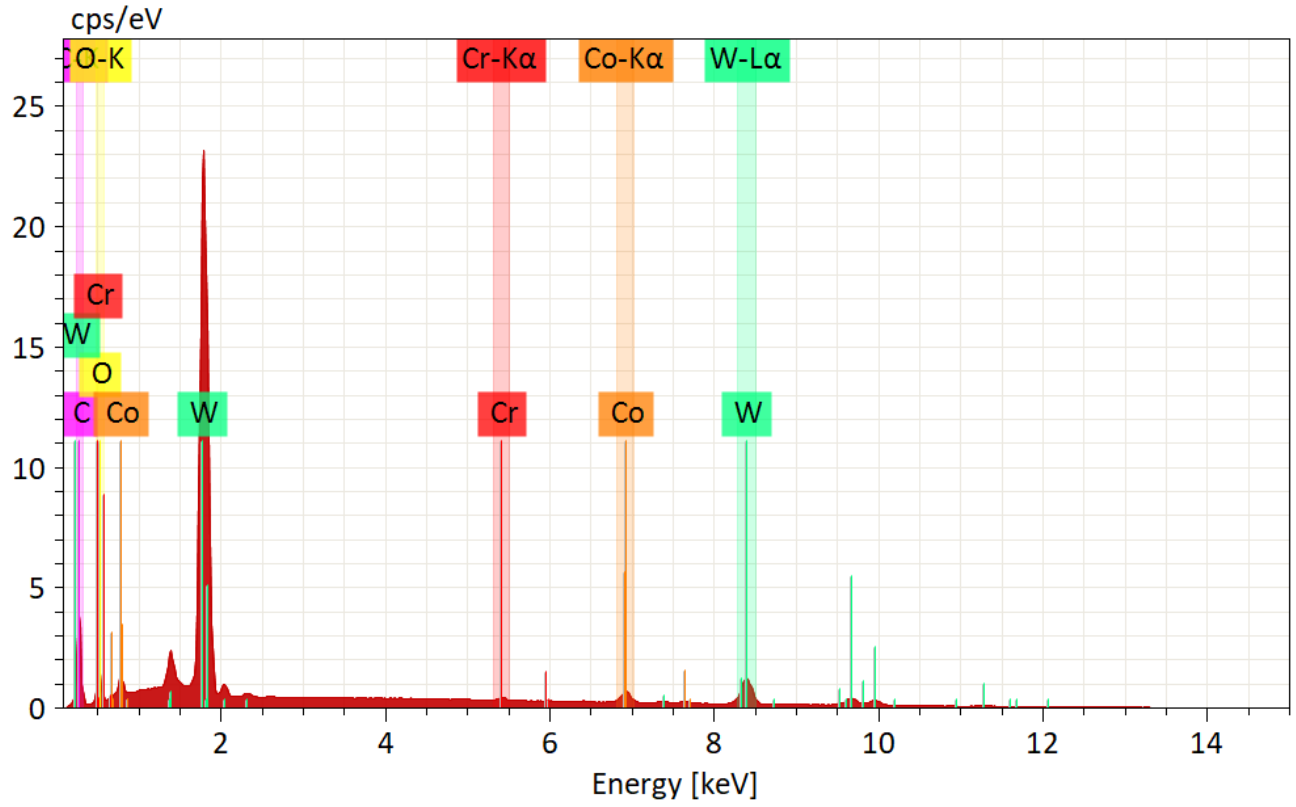


(b)

**Figure 36.** EDS over WC-CoCr eroded surface: (a) line scan compositional analysis: (b) EDS spectra.

Several important observation can be done using obtained results. Relative amount of carbon (purple color in the graphic of Figure 29-a) have risen significantly inside the eroded area, while relative amount of tungsten (blue-green color in the graphic of Figure 29-a) is decreased inside the eroded area. Binder elements cobalt and chromium have presented stable chemical evolution. Presence of oxygen over all the surface shows oxidation reaction happening on the surface of the specimens, more importantly, relative fraction of oxygen inside the eroded area is two times higher than outside, indicating the formation of oxides.

Several oxidation reactions are expected on the surfaces of WC-based composites with product of tungsten oxide, free carbon, etc. expected reaction are listed in the Equations 8-10.

$$2WC + O_2 \rightarrow 2WO_3 + 2C \quad (8)$$

$$WC + 3H_2O \rightarrow WO_3 + C + 3H_2 \quad (9)$$

$$WC + 3H_2O \rightarrow WO_3 + CH_4 + H_2 \quad (10)$$

Oxidation is preferable on the eroded area of the surfaces what is provided clearly with oxygen composition on the Figure 29-a.

The same can be observed by analysing Figure 30 representing the EDS mapping for an area where original surfaces (unworn) of the WC-CoCr specimen coexist with areas that have suffered cavitation-erosion, where once again it is possible to notice an increase in carbon and oxygen in the eroded areas which indicates the formation of oxides.

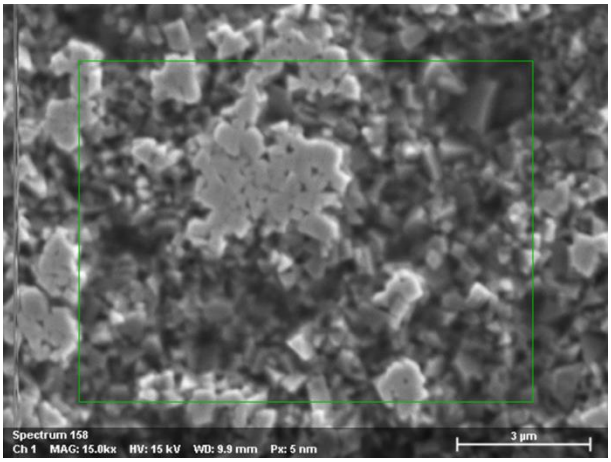


(a)

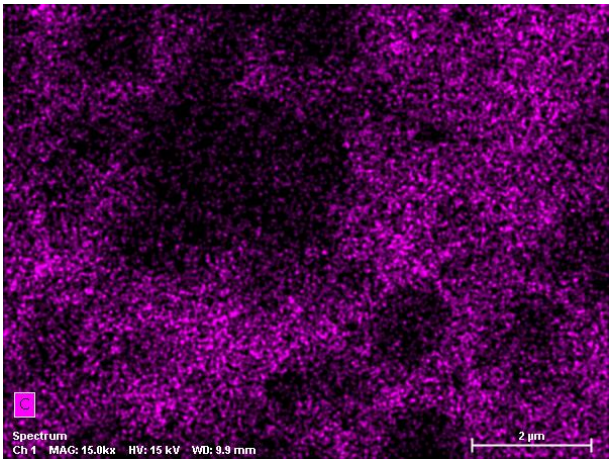


(b)

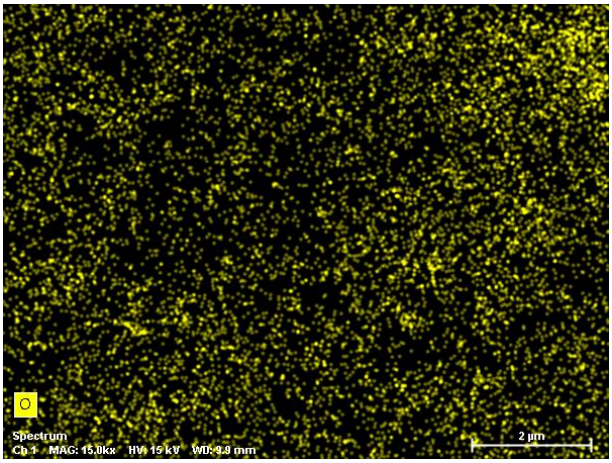


(c)

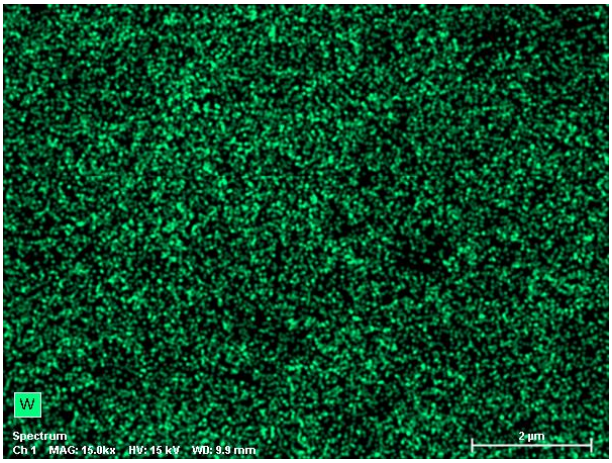


(d)

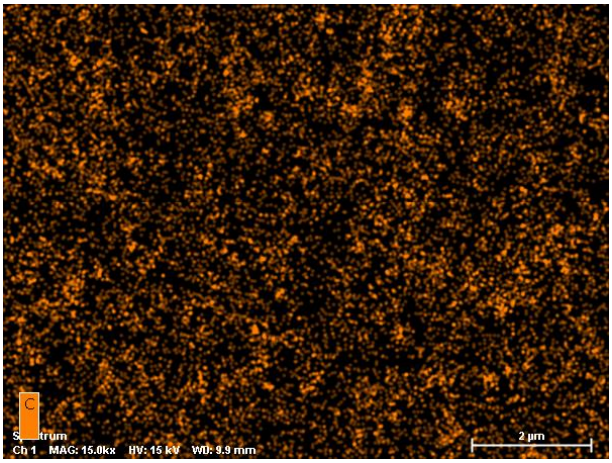


(e)

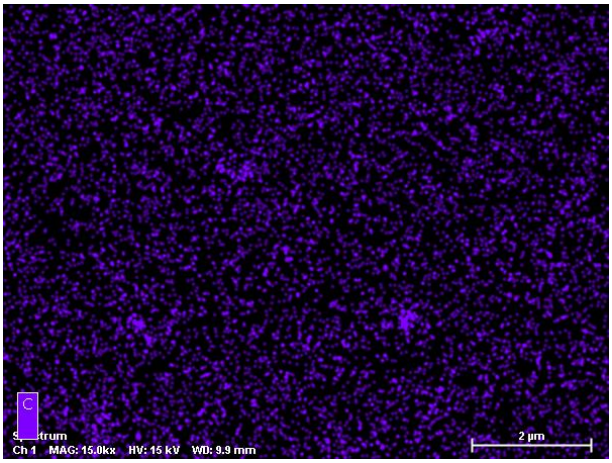


(f)

**Figure 30.** (a) SEM micrographs and EDS analysis for the WC-CoCr specimen, showing the map with the spectra of all the chemical elements: (b) carbon spectrum; (c) oxygen spectrum: (d) tungsten spectrum; (d) Cobalt spectrum and; (e) Chromium spectrum.

## 4.5 Subsurface hardening

Erosion evolution obtained from comparison of 2D profiles have shown several important features. From the graph shown in Figure 15 it is possible to observe that propagation of the erosion damage stops after a certain depth. There are several explanations that could be given to describe observed phenomena.

First, erosion of the specimen surface and counter body surface, changes the distance between the operating system (body and counterbody). Initially, distance between surfaces was set to 1 mm, the pit depth increases the working distance and therefore cavitation-erosion could have lower impact and damage rate slows down.

Second, continuous damage initiated with ultrasonic pressure waves initiates plastic deformation on the surface of the specimen. Hardening of the surface could slow down the damage rate.

Third, we can suggest that not all the surface undergoes changes due to plastic deformation, but the subsurface underneath the surface directly affected by cavitation damage. The stress field created by the ultrasonic device is not known and it suggests the possibility that maximum stress is created not on the surface, but on the subsurface. Subsurface hardening can be investigated with a cross-section analysis of the specimen. Secondary cracks could be attempted to be observed and the stress field could be defined more accurately.

# 5. Conclusion

WC-based composites with several different binders have been analyzed in the framework of this research investigation: WC-Co, WC-Ni, WC-CoNi, WC-CoCr, WC-NiCr, WC-CoNiCr and WC-NiCrMo have been studied using cavitation-erosion test method. Cavitation-erosion resistance have been calculated for each of the binder and erosion mechanism that have been analyzed.

The results of the undertaken work are as following:

- Volume loss rates have been calculated in order to compare different specimens' cavitation erosion resistance. Co binder CER is 0.00282 $mm^3$/hour, Ni CER is 8.90E-05 $mm^3$/hour, CoNi CER is 3.75E-05 $mm^3$/hour, CoCr CER is 1.11E-05 $mm^3$/hour, NiCr CER is 6.60E-07 $mm^3$/hour, CoNiCr CER is 2.82E-06 $mm^3$/hourNiCrMo, CER is 4.17E-06 $mm^3$/hour. Therefore, CER of the best performing binder NiCr was ~4000 times higher than the worst one Co.
- Cavitation erosion resistance of WC-NiCr have shown the best cavitation-erosion resistance. The order of binder performance from the best to the worst is as follows: NiCr, CoNiCr, NiCrMo, CoCr, CoNi, Ni, and Co. The best performance is given by binders with cobalt, next nickel, being the worst performance given by cobalt binder.
- Cavitation-erosion resistance and measured hardness values have provided strong correlation, given that better performance of harder composites.
- Volume loss rates have shown several stages of cavitation erosion. Accelerating and decelerating stages of cavitation erosion have been clearly observed.
- SEM analysis have revealed that erosion mechanism is driven by softer binder removal and complete undamaged grain detachment.
- Compositional analysis using EDS have revealed exceeding oxidation rate in the eroded area. Chromium and nickel binder composites have provided lower oxidation rate and higher cavitation erosion resistance, what let us suggest that oxidation takes one of central roles in erosion process.

# 6. Future work

The following future work is recommended to continue the development of the topic of cavitation erosion behavior of WC-based composites:

- Prepare and analyze WC-Cr composite, as chromium binder provided the best performance
- Analyze oxidation behavior of WC composites with different binders
- Analyze mutual corrosion/oxidation and cavitation erosion behavior
- Perform experiments with shorter time steps at the beginning of cavitation erosion and increase the overall duration of the experiment
- Perform cross-sectional hardness measurements of the composites after cavitation erosion
- Measure fraction of free carbon and tungsten trioxide on new surface
- Analyze hardness and integrity of new formed surface

# References

[1] Amann, T., Waidele, M. and Kailer, A., 2018. Analysis of mechanical and chemical mechanisms on cavitation erosion-corrosion of steels in salt water using electrochemical methods. Tribology International, 124, pp.238-246.

[2] Zakrzewska, D.E. and Krella, A., 2019. Cavitation erosion resistance influence of material properties. Advances in Materials Science, 19, pp.18-34.

[3] ASTM, N., 2003. Standard test method for cavitation erosion using vibratory apparatus. ASTM: West Conshohocken, PA, USA.

[4] Franc, J.P. and Michel, J.M., 2006. Fundamentals of cavitation (Vol. 76). Springer science & Business media.

[5] Young, F.R., 1999. Cavitation. World Scientific.

[6] B V Hubballi, D.V., 2013. A review on the prediction of cavitation erosion inception in hydraulic control valves.

[7] Dular, M., Požar, T. and Zevnik, J., 2019. High speed observation of damage created by a collapse of a single cavitation bubble. Wear, 418, pp.13-23.

[8] Szala, M. and Hejwowski, T., 2018. Cavitation erosion resistance and wear mechanism model of flame-sprayed Al2O3-40% TiO2/NiMoAl cermet coatings. Coatings, 8(7), p.254.

[9] Tzanakis, I., Bolzoni, L., Eskin, D.G. and Hadfield, M., 2017. Evaluation of cavitation erosion behavior of commercial steel grades used in the design of fluid machinery.

[10] Ding, X.; Ke, D.; Yuan, C.-Q.; Ding, Z.-X.; Cheng, X.-D. Microstructure and cavitation erosion resistance of HVOF deposited WC–Co coatings with different sized WC. Coatings 2018, 8, 307.

[11] Du, J., Zhang, J. and Zhang, C., 2019. Effect of heat treatment on the cavitation erosion performance of WC–12Co coatings. Coatings, 9(10), p.690.

[12] Tam, K.F., Cheng, F.T. and Man, H.C., 2002. Cavitation erosion behavior of laser-clad Ni–Cr–Fe–WC on brass. Materials Research Bulletin, 37(7), pp.1341-1351.

[13] Hutchings, I. and Shipway, P. (2017) Tribology: Friction and wear of engineering materials: Second Edition, Tribology: Friction and Wear of Engineering Materials: Second Edition.

[14] Hammitt, F. G. (1979) 'CAVITATION EROSION: THE STATE OF THE ART AND PREDICTING CAPABILITY.', Appl Mech Rev.

[15] Rao, A. S. and Kung, D. (1987) METALLIC OVERLAY MATERIALS FOR THE OPTIMUM CAVITATION PERFORMANCE OF HYDRAULIC TURBINES., Research and Development Report - Canadian Electrical Association.

[16] Karimi, A. (1989) 'Cavitation erosion of austenitic stainless steel and effect of boron and nitrogen ion implantation', Acta Metallurgica.

[17] Xiaojun, Z. et al. (2003) 'Phase transformation during cavitation erosion of a Co stainless steel', Materials Science and Engineering A.

[18] Padilha, A., 2000. Materiais De Engenharia: Microestrutura E Propriedades. São Paulo (SP): HEMUS.

[19] J.S. Rinehart, J. Pearson, Behavior of Metals under Impulsive Loads, American society for metals, Cleveland, Ohio, 1954.

[20] National Oceanic and Atmospheric Administration (NOAA). Shipping noise and marine mammals: A forum for science, management, and technology. Report, Arlington, VA, USA, May 2004.

[21] Lauterborn, W., 1980. Cavitation and coherent optics. In Cavitation and inhomogeneities in underwater acoustics (pp. 3-12). Springer, Berlin, Heidelberg.

[22] Euler, L. (1755) 'Principes generaux du mouvement des fluides', Histoire de l'Académie Royale des Sciences et des Belles-Lettres de Berlin.

[23] Gopalan, S., Katz, J. and Knio, O., 1999. The flow structure in the near field of jets and its effect on cavitation inception. Journal of fluid mechanics, 398, pp.1-43.

[24] Shah Y. T., Pandit A. B., Moholkar V. S., (1999) - Cavitation Reaction Engineering- Springer US.

[25] Bai, L.X., Xu, W.L., Zhong, T. and Li, N.W., 2008. A high-speed photographic study of ultrasonic cavitation near rigid boundary. Journal of Hydrodynamics, Ser. B, 20(5), pp.637-644.

[26] Gu, J., Luo, C., Zhou, W., Tong, Z., Zhang, H., Zhang, P. and Ren, X., 2020. Degradation of Rhodamine B in aqueous solution by laser cavitation. Ultrasonics Sonochemistry, 68, p.105181.

[27] Chudina, M., 2003. Noise as an indicator of cavitation in a centrifugal pump. Acoustical physics, 49(4), pp.463-474.

[28] ASTM, N., 2016. ISO 4499-4:2016 Hardmetals — Metallographic determination of microstructure — Part 4: Characterisation of porosity, carbon defects and eta-phase contentASTM: West Conshohocken, PA, USA.

[29] Heideman, M., Johnson, D. and Burrus, C., 1984. Gauss and the history of the fast Fourier transform. IEEE ASSP Magazine, 1(4), pp.14-21.

[30] Haosheng, C. and Shihan, L., 2009. Inelastic damages by stress wave on steel surface at the incubation stage of vibration cavitation erosion. Wear, 266(1-2), pp.69-75.

[31] Honarvar, F. and Varvani-Farahani, A., 2020. A review of ultrasonic testing applications in additive manufacturing: Defect evaluation, material characterization, and process control. Ultrasonics, p.106227.

[32] 250 - 450 Sonifier Analog Cell Disruptor User's Manual EDP 100-413-016 Rev. C BRANSON Ultrasonics Corporation 41 Eagle Road Danbury, Connecticut 06813-1961 U.S.A.

[33] Pereira, P., Vilhena, L.M., Sacramento, J., Senos, A.M.R., Malheiros, L.F. and Ramalho, A., 2021. Abrasive wear resistance of WC-based composites, produced with Co or Ni-rich binders. Wear, p.203924.